AD-A093 305 OHIO STATE UNIV COLUMBUS ELECTROSCIENCE LAB F/G 9/5
A HYBRID METHOD OF MOMENTS TECHNIQUE FOR COMPUTING ELECTROMAGNE--ETC(U)
APR 80 S DAVIDSON, G THIELE N00014-78-C-0049
UNCLASSIFIED ESL-710816-8 NL

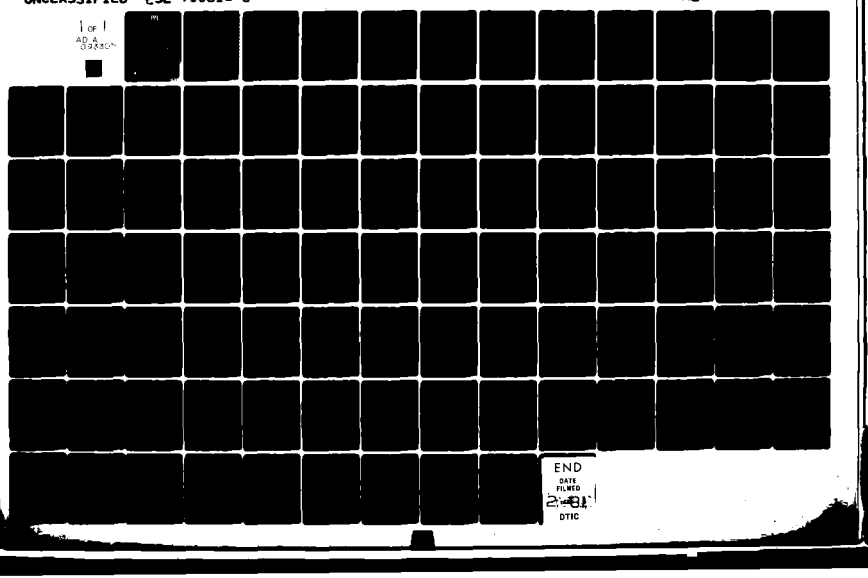

LEVEL II

A HYBRID METHOD OF MOMENTS TECHNIQUE FOR COMPUTING ELECTROMAGNETIC COUPLING BETWEEN TWO MONOPOLE ANTENNAS ON A LARGE CYLINDRICAL SURFACE

The Ohio State University

S. A. Davidson
G. A. Thiele

The Ohio State University

ElectroScience Laboratory

Department of Electrical Engineering
Columbus, Ohio 43212

TECHNICAL REPORT 710816-8

Contract N00014-78-C-0049

April 1980

Dept. of the Navy
Office of Naval Research
Arlington, Virginia 22217

NOTICES

When Government drawings, specifications, or other data are used for any purpose other than in connection with a definitely related Government procurement operation, the United States Government thereby incurs no responsibility nor any obligation whatsoever, and the fact that the Government may have formulated, furnished, or in any way supplied the said drawings, specifications, or other data, is not to be regarded by implication or otherwise as in any manner licensing the holder or any other person or corporation, or conveying any rights or permission to manufacture, use, or sell any patented invention that may in any way be related thereto.

SECURITY CLASSIFICATION OF THIS PAGE *(When Data Entered)*

REPORT DOCUMENTATION PAGE

READ INSTRUCTIONS BEFORE COMPLETING FORM

1. REPORT NUMBER	2. GOVT ACCESSION NO. AD-A093305 (9)
	3. RECIPIENT'S CATALOG NUMBER
4. TITLE *(and Subtitle)* (6) A HYBRID METHOD OF MOMENTS TECHNIQUE FOR COMPUTING ELECTROMAGNETIC COUPLING BETWEEN TWO MONOPOLE ANTENNAS ON A LARGE CYLINDRICAL SURFACE.	5. TYPE OF REPORT & PERIOD COVERED TECHNICAL REPORT. (13)
	6. PERFORMING ORG. REPORT NUMBER (14) ESL-710816-8
7. AUTHOR(s) (10) S.A. Davidson and G.A. Thiele	8. CONTRACT OR GRANT NUMBER(s) Contract N00014-78-C-0049 (15)
9. PERFORMING ORGANIZATION NAME AND ADDRESS The Ohio State University ElectroScience Laboratory, Department of Electrical Engineering, Columbus, Ohio 43212	10. PROGRAM ELEMENT, PROJECT, TASK AREA & WORK UNIT NUMBERS Project NR 371-021/9-5-78 (427)
11. CONTROLLING OFFICE NAME AND ADDRESS Dept. of the Navy, Office of Naval Research, 800 Quincy Street Arlington, VA 22217 (11)	12. REPORT DATE April 1980
	13. NUMBER OF PAGES 86
14. MONITORING AGENCY NAME & ADDRESS *(if different from Controlling Office)* (12) 91	15. SECURITY CLASS. *(of this report)* Unclassified
	15a. DECLASSIFICATION/DOWNGRADING SCHEDULE

16. DISTRIBUTION STATEMENT *(of this Report)*

DISTRIBUTION STATEMENT A
Approved for public release;

17. DISTRIBUTION STATEMENT *(of the abstract entered in Block 20, if different from Report)*

18. SUPPLEMENTARY NOTES

19. KEY WORDS *(Continue on reverse side if necessary and identify by block number)*

Moment method
Diffraction theory
Geometrical Theory of Diffraction
Hybrid technique
Mutual coupling
Antennas
Electromagnetic scattering

20. ABSTRACT *(Continue on reverse side if necessary and identify by block number)*

The hybrid technique presented in this paper is a method for solving electromagnetic problems in which an antenna or other discontinuity is located on or near a conducting body, such as antennas on aircraft or ships. The technique solves these kinds of problems by properly analyzing the interaction between the antenna or scatterer and the conducting body. The hybrid technique accomplishes this by casting the antenna structure in a moment method format and then modifying that format to account for the effects of the conducting body via the

DD FORM 1 JAN 73 1473 EDITION OF 1 NOV 65 IS OBSOLETE

402251

SECURITY CLASSIFICATION OF THIS PAGE *(When Data Entered)*

20. ABSTRACT (con't)

geometrical theory of diffraction (GTD). The technique extends the moment method to handle many problems that cannot be solved by GTD or the moment method alone.

In general, arbitrary radiators located on or near canonical shapes or combinations thereof can be solved using the hybrid technique. Electromagnetic parameters which the hybrid technique can solve for include the near and far fields, current distributions, impedances, and scattering data. In this paper, a transmitting and receiving monopole antenna, located on the surface of a perfectly-conducting circular cylinder, are analyzed to determine the amount of radiated power which arrives at the receiving antenna, after accounting for the reflection and curved surface diffraction effects of the conducting cylinder.

The purpose of this paper is to present the technique and to demonstrate some of its facility and its accuracy, as evidenced by the close agreement of its results to the results of an electromagnetic computer analysis program currently used by the United States Air Force (USAF) solving similar problems. Using both computer programs, antennas are modeled as one-quarter wavelength monopoles and are positioned on conducting circular cylinders with radii ranging from one to 150 wavelengths. The power coupling between the antennas is computed by both computer codes and graphed as a function of the separation between the antennas. The near-perfect agreement in the results of these radically different analysis codes implies that their solutions, in general, are correct.

CONTENTS

CHAPTER I

INTRODUCTION

The wide-spread availability of very large, rapid digital computer systems has lead to the use of two fundamental methods of modeling the electromagnetic characteristics of wire antennas on or near three-dimensional metallic surfaces. One technique is known as the method of moments whereby the interaction between electromagnetic fields and their induced currents on the wire antenna as well as on all parts of nearby conducting bodies, modeled as wire grids or flat plates, is computed. Consequently, this approach, which computes the electromagnetic field from a wire antenna, is significantly limited by computer storage and is only practical when the nearby conducting bodies are on the order of a few wavelengths in size. An alternative approach is to use the geometrical theory of diffraction (GTD) which requires that more assumptions about the problem be made, such as the radiation pattern generated by the antenna, but may be applied to bodies that are arbitrarily large in an electrical sense. Much work has been done in the recent past to combine the method of moments with the GTD in a hybrid fashion so as to overcome the disadvantages of these techniques when used separately.

The purpose of this thesis is two fold. First, the idea of a hybrid technique of combining the method of moments with GTD is

entended to account for the mutual coupling between two monopole antennas on a large circular cylinder by means of curved surface wave diffraction. Second, the results of this technique are compared to those of an analysis program used by the United States Air Force which predicts electromagnetic coupling between aircraft antennas. The close agreement between the results of these two different analysis techniques serves to validate both computer programs.

The basic hybrid technique used in this paper was first described in the literature by Thiele and Newhouse [1]. There, the technique was applied to antennas on and near finite planar surfaces. Wedge diffraction theory was combined with the method of moments to account for the finite planar surfaces. Ekelman [2], building on this previous work, developed a hybrid technique for combining the moment method treatment of wire antennas with the GTD to account for reflection of electromagnetic energy from the curved surface of an infinitely long cylinder as well as diffraction from the ends of a finite cylinder. In the present paper, curved surface diffraction theory is used to extend a method of moments thin-wire analyses program to account for the propagation of electromagnetic energy around the curved surface of an infinitely long cylinder.

CHAPTER II

METHOD OF MOMENTS THEORY

In this chapter, a fairly detailed description of the moment method theory is presented which serves as a foundation for the hybrid technique presented in Chapter IV. Since this paper is a technique for extending a moment method analysis program, an extensive discussion of the method of moments is considered appropriate.

The method of moments is a procedure for reducing an integral equation of the form

$$\int_{\text{over structure}} I(z')K(z,z')dz' = -E^{i} \tag{2-1}$$

to a system of simultaneous linear algebraic equations in terms of the unknown current $I(z')$. It can be used to determine the current distribution on an antenna, based on the physical properies of the antenna, its configuration, and even possible environmental influences such as the presence of a nearby conducting surface. Thus the traditional problem in antenna theory of deriving the form of the current distribution on the antenna is solved. Once the current is known, radiation patterns and impedance can be determined in a straightforward manner.

The specific computer code used for the moment method portion of the analysis is based on the thin-wire program written by Richmond [3]. It requires that all antennas and scatterers consist of thin wires or a

grid of thin wires. This constraint allows one to make use of Pocklington's integral equation to describe the relationship between an electric field incident on the surface of a wire and the resulting surface current induced on the wire. Details of the derivation of the Pocklington integral equation are given by Stutzman and Thiele [4]. The general form of the Pocklington integral equation for a wire of length L whose axis is parallel to the z axis is given by

$$(2\text{-}2)\quad \int_{-L/2}^{L/2} I(z') \left[\frac{\partial^2 G(z,z')}{\partial z^2} + k^2 G(z,z') \right] \frac{dz'}{j\omega\varepsilon} = - E_z^i(z)$$

where

$G(z,z')$ = free space Green's function = $\dfrac{e^{-jkr}}{4\pi r}$

$r = \left[a^2 + (z-z')^2 \right]^{1/2}$

a = wire radius

$I(z')$ = filamentary line current on the axis of the wire equivalent to the induced surface current integrated around the circumference of the wire

k = wave number of the medium = $\dfrac{2\pi}{\lambda} = \omega\sqrt{\mu\varepsilon}$

The parameters ω and λ are the angular frequency and wavelength respectively, and μ and ε are the permeability and permittivity of the medium surrounding the wire.

Equation (2-2) is based on several key assumptions. First, the wire is assumed to be "thin"; the wire radius, a, must be much less than a wavelength. Therefore, it is assumed that only axially directed currents (z-axis) are present. Secondly, the conductivity of the wire is assumed to be infinite, and therefore, all induced current resides on the surface of the wire. Since the radius of the wire is small,

this surface current, $J(z',\theta)$, is uniform around the circumference of the wire at any given point along the wire. Therefore, by symmetry this surface current can be replaced by a line current which is located on the axis of the wire. That is

$$(2\text{-}3) \quad I(z') = \int_0^{2\pi} J(z',\theta)a\,d\theta$$

It is important to note that eqn. (2-2) is in the form of eqn. (2-1) so that eqn. (2-2) may be rewritten as

$$(2\text{-}4) \quad \int_{-L/2}^{L/2} I(z')K(z_m,z')dz' = -E_z^i(z_m)$$

A physical interpretation of eqn. (2-4) is that an electric field incident on the surface of the wire at point z_m along the wire axis, will induce a surface current equivalent to a line current distribution $I(z')$ located on the axis of the wire over a length L as shown in Fig. 2-1.

At this point, it is necessary to consider the boundary conditions at the surface of the wire. From classical electromagnetic theory, at the surface of a boundary on which there is an incident field, one must account for a transmitted field and a scattered field as shown in Fig. 2-2. The relationship between these three tangential fields at the boundary, $z = z_o$, is

$$(2\text{-}5) \quad E^i + E^s = E^t$$

However, a time varying field cannot exist in a perfect conductor and since the wire is assumed to be a perfect conductor, the boundary condition on the tangential fields at the wire surface becomes

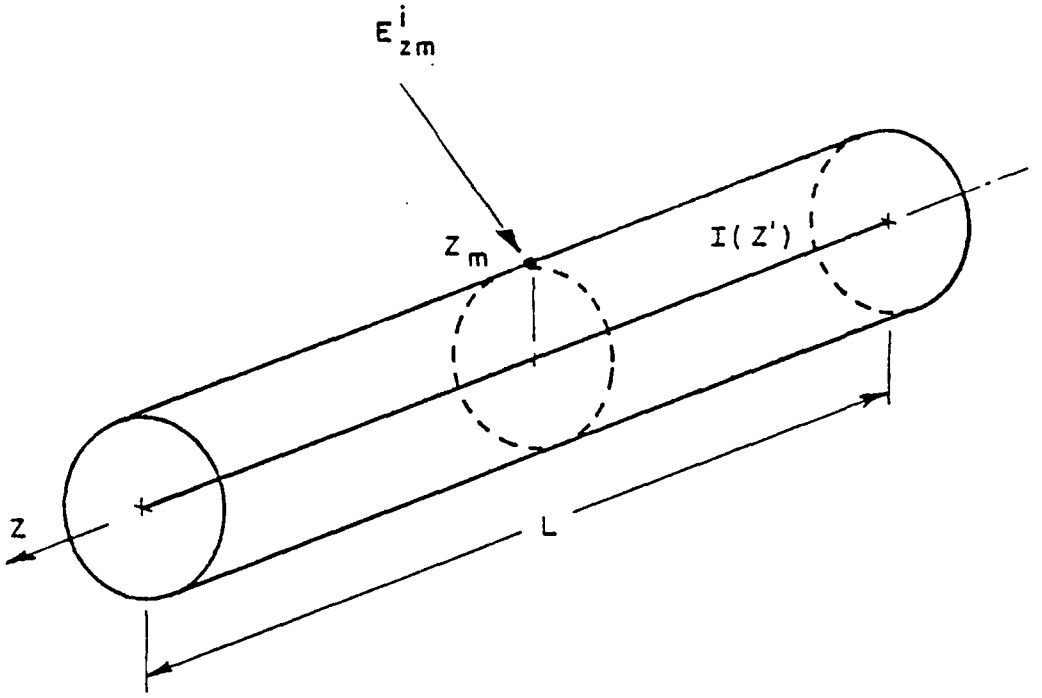

Fig. 2-1. Equivalent axial wire current induced by a incident field

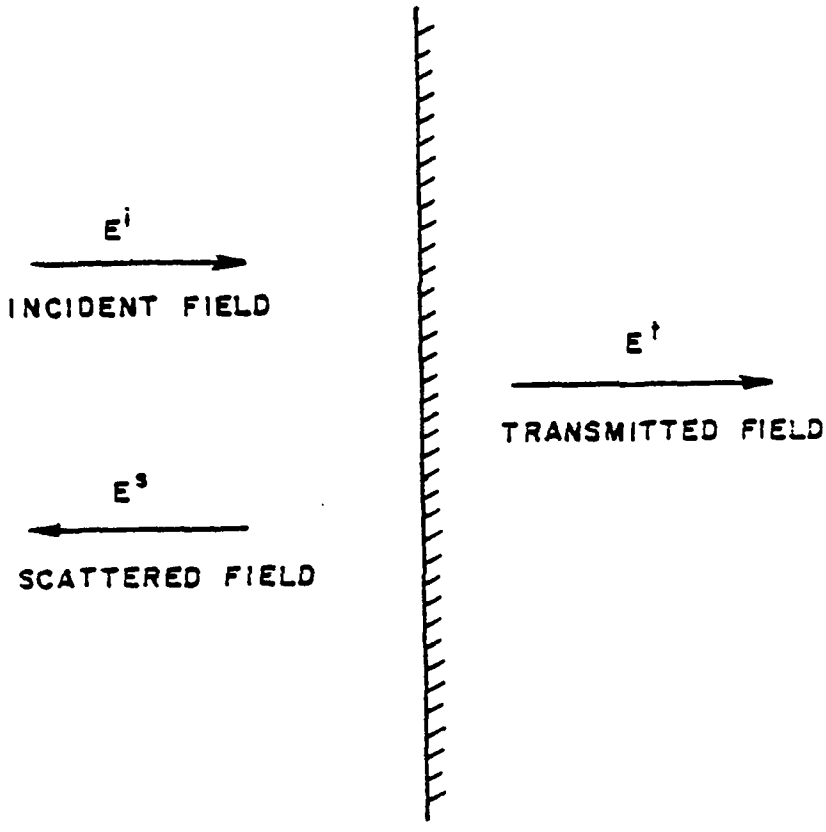

Fig. 2-2. Boundary conditions

(2-6) $E^i + E^s = 0$

Eq . (2-5) can be rewritten as

(2-7) $E^s = - E^i$

Finally, combining eqn. (2-6) with eqn. (2-4), yields

$$(2\text{-}8) \quad \int_{-L/2}^{L/2} I(z')K(z_m,z')dz' = E^s(z_m)$$

A physical interpretation of eqn. (2-8) is that a line current $I(z')$ located on the axis of a "wire" of length L produces a field $E^s(z)$ at an observation point z on the surface of the "wire" as illustrated in Fig. 2-3.

The next important step in the moment method concept is to divide the wire of length L into N segments of length Δz_n. This allows one to write eqn. (2-4) as

$$(2\text{-}9) \quad - E_z^i(z_m) = \int_{-L/2}^{L/2} I(z')K(z_m z')dz' = \sum_{n=1}^{N} I_n \int_{\Delta z} F_n K(z_m,z')dz'$$

where the current function over the wire, $I(z')$, is now represented as a series of current magnitudes at each segment n, (I_n), multiplied by a function which describes the shape of the current for each n segment. F_n is referred to in the literature as the <u>expansion function</u>. For example, if one chose to make the current constant for each segment, thereby forming a current function $I(z')$ along the wire consisting of a series of rectangular pulses, F_n could be written as an orthogonal pulse function. Therefore,

$$(2\text{-}10) \quad I(z') = \sum_{n=1}^{N} I_n F_n$$

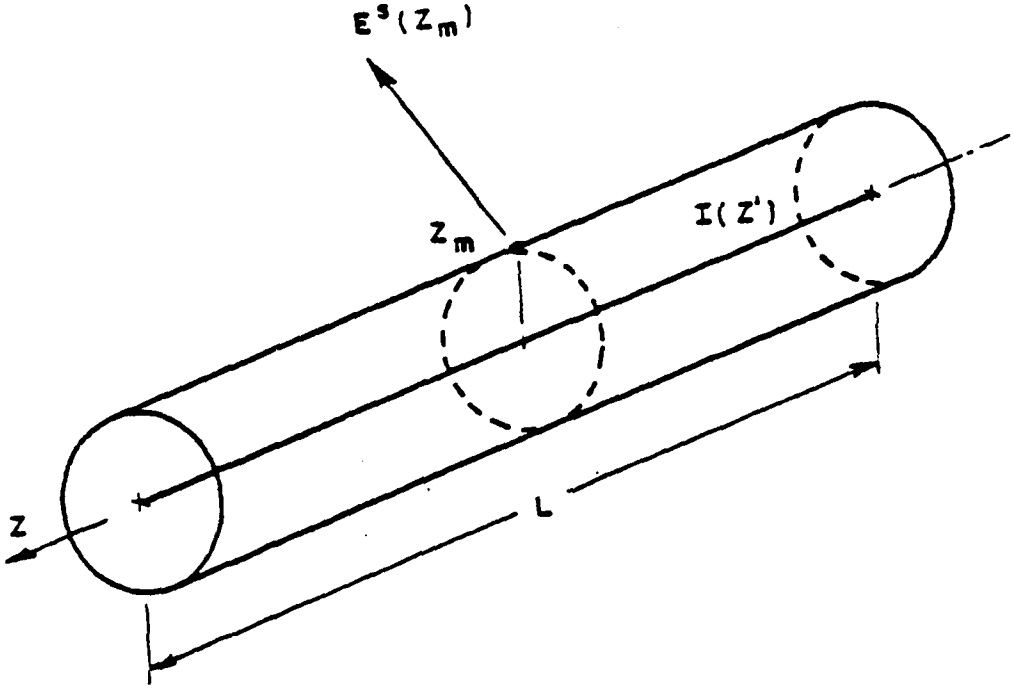

Fig. 2-3. Scattered field induced by an equivalent axial wire current

where

$$(2\text{-}11)\quad F_n = \begin{cases} 1 & \text{for } z' \text{ in } \quad z_n' \\ 0 & \text{otherwise} \end{cases}$$

For illustrative purposes, let us choose the orthogonal pulse function as the expansion function. This permits factoring constants out of the integral and eqn. (2-9) can be rewritten as

$$(2\text{-}12)\quad -E_z^i(z_m) = \int_{-L/2}^{L/2} \left(\sum_{n=1}^{N} I_n F_n \right) K(z_m, z')dz' =$$

$$\sum_{n=1}^{N} I_n \int_{\Delta z_n'} K(z_m, z_n')dz'$$

Evaluating the integral on the right-hand side of eqn. (2-12),

$$(2\text{-}13)\quad \int_{\Delta z_n'} K(z_m, z_n')\, dz' = C(z_m, z_n')\ \Delta z'$$

Thus, eqn. (2-12) can be written as

$$(2\text{-}14)\quad -E_z^i(z_m) = \int_{-L/2}^{L/2} \left(\sum_{n=1}^{N} I_n F_n \right) K\,(z_m, z')\, dz' =$$

$$\sum_{n=1}^{N} I_n\, C\,(z_m, z_n')\ \Delta z'$$

Combining eqn. (2-14) with eqns. (2-9), (2-8), and (2-7)

$$(2\text{-}15)\quad E_z^s(z_m) = \int_{-L/2}^{L/2} I(z')K(z,z')dz' = \sum_{n=1}^{N} I_n C(z_m, z_n')\ \Delta z'$$

$$= I_1 C(z_m, z_1')\,\Delta z' + I_2 C(z_m, z_2')\,\Delta z + \ldots$$

$$+ I_n C(z_m, z_n')\,\Delta z' + \ldots + I_N C(z_m, z_N')\,\Delta z' = -E_z^i(z_m)$$

The physical interpretation of eqn. (2-15) is as follows [4]. The wire has been divided into N segments of length $\Delta z'$ with the current being an unknown constant over each segment (due to our choice of the expansion function F). At the center of the m^{th} segment, the sum of the scattered fields from all of the N segments is set equal to the negative of the incident field at the point z_m (eqn. 2-7). The incident field is a known field due to a source located on the wire (transmitting case) or a source not located on the wire (receiving case).

By examining eqn. (2-15), one may notice that it resembles Kirchhoff's network equations

$$(2\text{-}16) \quad \sum_{n=1}^{N} Z_{mn} I_n = V_m, \qquad m = 1,2,3,\ldots N$$

with which most electrical engineers are more familiar (and comfortable), where

$$(2\text{-}17) \quad Z_{mn} = C(z_m, z_n')\Delta z$$

$$V_m = - E_z^i(z_m)$$

Since $C(z_m, z_n')\Delta z$ is based on the geometry of the wire and V_m is given for all m, the values for I_n can be determined by n independent equations. In addition, the boundary condition of eqn. (2-6) shall be enforced at the center of each of the n segments. This is referred to as point-matching which is a special case of more general moment methods. Point matching results in the following system of equations.

$$(2\text{-}19) \quad \begin{aligned} I_1 C(z_1, z_1')\Delta z' + I_2 C(z_1, z_4')\Delta z' + \ldots + I_N C(z_1, z_N') &= -E_2^i(z_1) \\ I_1 C(z_2, z_1')\Delta z' + I_2 C(z_2, z_2')\Delta z' + \ldots + I_N C(z_2, z_N') &= -E_2^i(z_2) \\ \vdots \qquad\qquad \vdots \qquad\qquad \vdots \qquad\qquad & \vdots \\ I_1 C(z_N, z_1')\Delta z' + I_2 C(z_N, z_2')\Delta z' + \ldots + I_N C(z_N, z_N') &= -E_z(z_N) \end{aligned}$$

which can be written in compact matrix notation as

$$(2\text{-}20) \quad [I_n]\,[C(z_{m,n})\Delta z'] = [-E^i_z(z_n)]$$

Making use of eqns. (2-17) and (2-18), eqn. (2-20) can be rewritten as:

$$(2\text{-}21) \quad [I_n]\,[Z_{m,n}] = V_m$$

Finally, the desired solution is obtained from eqn. (2-21) symbolically as:

$$(2\text{-}22) \quad (I_n) = [Z_{m,n}]^{-1}\,[V_m]$$

In practice, one does not explicitly generate $[Z_{m,n}]^{-1}$, but instead may solve eqn. (2-21) by using several fairly standard matrix algorithms which utilize properties of the Z_{mn} matrix such as its diagonal symmetry.

Another important concept of the method of moments is weighted residuals. As the reader may recall, the point-matching method enforces the boundary condition of eqn. (2-6) only at the midpoint of any segment on the wire. At points other than the midpoint, z_m, of a segment, eqn. (2-6) becomes

$$(2\text{-}23) \quad E^s_{tan} + E^i_{tan} = R$$

where R is referred to as the residual. Thus, when R does not equal zero, the boundary condition is violated; the more severely this boundary condition is violated, the greater will be the chance that the final solution for the currents will be incorrect. By combining eqn. (2-23) with eqns. (2-8) and (2-9)

$$(2\text{-}23) \quad R = \sum_{n=1}^{N} I_n \int_{\Delta z_n} F_n K(z_m, z')\,dz' + E^i_{z_m}(z_m)$$

and for orthogonal pulse expansion functions,

$$R = \sum_{n=1}^{N} I_n C(z_m, z_n') \Delta z' + E_z^i(z_m)$$

In the method of weighted residuals, a current function $I(z')$ is chosen so as to force the residual to zero in an average sense [4]. This can be mathematically expressed as

$$(2\text{-}24) \quad \int_{-L/2}^{L/2} W_m R \, dz = 0, \qquad m = 1,2,3,\ldots,N$$

where W_m is referred to as a weighting or testing function. Substituting eqn. (2-23) into eqn. (2-24) gives, in general:

$$(2\text{-}25) \quad \int_{-L/2}^{L/2} W_m \sum_{n=1}^{N} I_n \int_{\Delta z_m} F_n K(z_m, z') dz' dz + \int_{-L/2}^{L/2} W_m E_z^i(z_m) dz = 0$$

and for the orthogonal rectangular expansion function,

$$(2\text{-}26) \quad \int_{-L/2}^{L/2} \left(W_m \cdot \sum_{n=1}^{N} I_n C(z_m, z_n') \Delta z' \right) k + \int_{-L/2}^{L/2} W_m \cdot E_z^i(z_m) dz = 0$$

The point-matching method of enforcing the boundary condition at segment midpoints amounts to using the dirac delta function

$$(2\text{-}27) \quad W_m = \delta(z - z_m)$$

where

$$\int_{-\infty}^{\infty} \delta(z - z_m) dz = 1$$

and eqn. (2-26) reduces to the expressions in eqn. (2-15).

In the previous discussion, the orthogonal pulse and dirac delta function were chosen for the expansion and the weighting function so as

to keep the mathematical expressions as simple as possible. However, experience has shown that it is desirable to choose an expansion function which will closely resemble the anticipated form of the current and to use that same function as the weighting function. When the expansion and weighting functions are chosen to be the same, the procedure is referred to as Galerkin's method. Since the current distribution on thin wire antennas is generally sinusoidal, it follows that the use of sinusoidal expansion and weighting functions leads to high accuracy with many fewer segments required than if the point-matching method is used. Fewer segments results in fewer segment currents (I_n) and therefore, a fewer number of independent equations to solve. This in turn yields a significant savings in computer memory and execution time required.

The thin-wire program written by Richmond is based on Galerkin's method utilizing piecewise sinusoidal expansion and weighting functions. This is the method and computer program upon which this thesis is built and which extends the class of problems which the computer program can handle.

CHAPTER III

GEOMETRIC THEORY OF DIFFRACTION - APPLICATION FOR A SMOOTH CONVEX SURFACE

The purpose of this chapter is to introduce a high frequency method, the geometrical theory of diffraction (GTD), which is applicable to bodies that are electrically large. This chapter will then discuss the use of GTD to determine the propagation of electromagnetic energy over the curved surface of a circular cylinder.

GTD views the propagation of electromagnetic energy as rays (analogous to rays of light) which are subject to scattering and diffraction from specific parts of a body such as flat surfaces, curved surfaces, or sharp edges. Unlike the method of moments, GTD only requires detailed information about the interacting body at points of reflection and diffraction. Thus, unlike the method of moments, the complexity and magnitude of the analysis does not increase as the electrical size of the interacting body increases. However, GTD relies on the use of more assumptions than the method of moments; primarily, the ray-like behavior of electromagnetic energy, which tends to render this method useless at very low frequencies.

The remainder of this chapter will focus on the diffraction which occurs at the surface of a perfectly conducting circular cylinder.

In conventional GTD analysis, the total field exterior to a curved surface will consist of incident, reflected, and diffracted rays which may be divided into five separate regions as shown in Fig. 3-1 [5]. The shaded Region II in the vicinity of the shadow boundary is a transition region which divides the lit zone from the shadow zone. Very close to the surface, Region II is subdivided into Regions IV and VI in the shadow and lit zone respectively. Region V is a subdivision of Region III which is in the immediate vicinity of the surface. More specifically, Regions IV and V are close to the portion of the surface which is a caustic of the surface diffracted rays; whereas, Region II is in the vicinity of the point of grazing incidence (Q_1) which is a caustic of the reflected ray. Regions IV, V and VI are therefore commonly referred to as the caustic or surface boundary layer regions. The curved surface diffraction hybrid analysis developed in this paper will be exclusively for this surface boundary layer.

The theory and equations which describe electromagnetic behavior in the surface boundary layer of an arbitrary, perfectly-conducting convex surface are explained by Pathak and Wang [6]. For the sake of brevity, this chapter will simply present the equations used to predict the electric field strength in the surface boundary layer from an infinitesimal electric current (or current moment) which is also located within the surface boundary layer. According to equ. (31) in Ref. [8], the electric field strength from a source at point P' which is observed at point P (see Fig. 3-2) is given by the following expression:

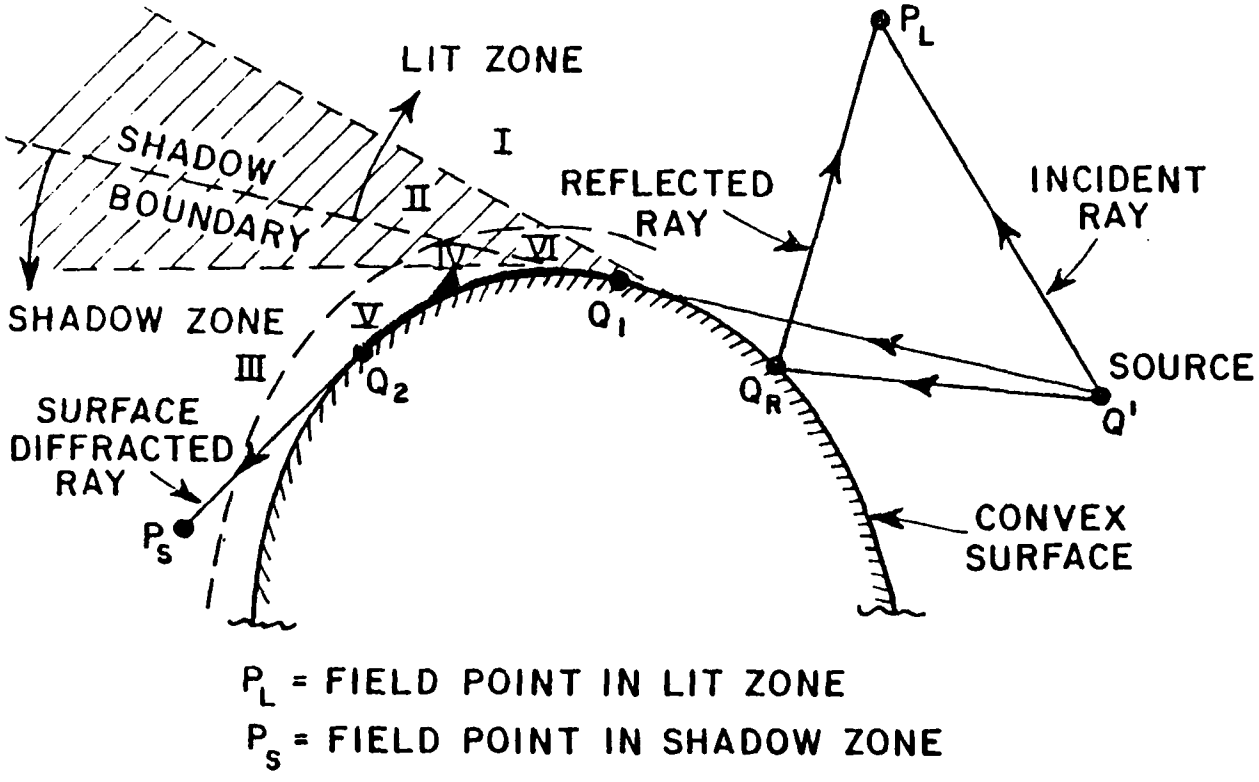

Fig. 3-1. The rays and regions associated with scattering by a smooth convex cylinder

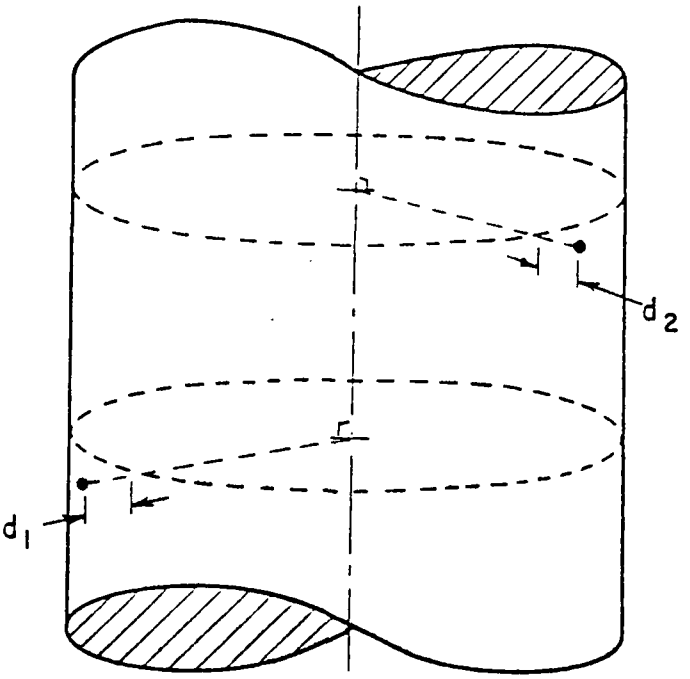

(a) SIDE VIEW

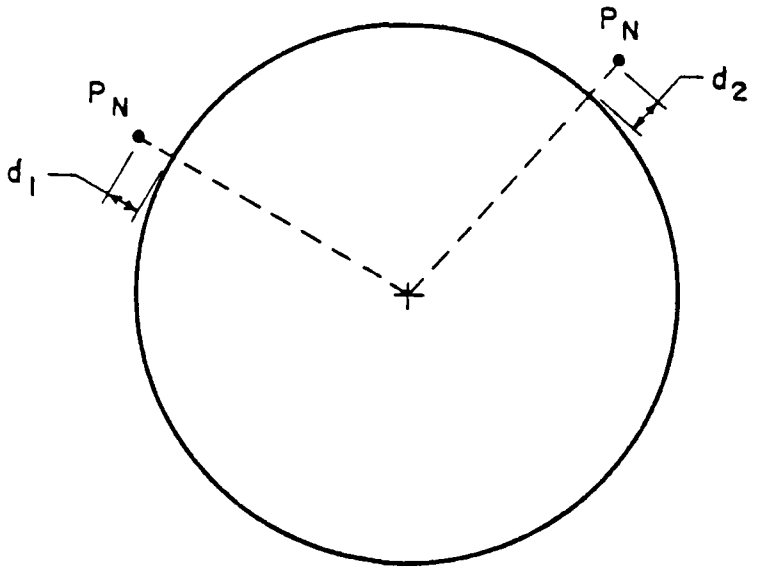

(b) END VIEW

Fig. 3-2. Circular Cylinder Geometry

$$(3\text{-}1)\quad \bar{E}_n^{\,e}(P) = z_o^2 DG(k_s)\bar{p}_e \cdot \hat{n}'\,\hat{n}$$
$$\left(\left\{F_n(\xi, y_1, y_2) - \frac{j}{k_s} F_h(\xi, y_1, y_2) + \left|\frac{j}{k_s}\right|^2 F_s(\xi, y_1, y_2)\right\} + \right.$$
$$\left. + T_o^{\,2} \frac{j}{k_s}\left\{F_s(\xi, y_1, y_2) - F_h(\xi, y_1, y_2)\right\}\right)$$

where

z_o = impedance of the medium = $\eta = \sqrt{\mu/\varepsilon}$

k = wavenumber of the medium = $2\pi/\lambda = \omega\sqrt{\mu\varepsilon}$

s = length of the surface ray geodesic path from P' to P

ρ_g = radius curvature of surface along the ray = $\dfrac{a}{\sin^2\delta}$

δ = angle of path with respect to the cylinder axis

a = cylinder radius

$$G(k_s) = \frac{ke^{-jks}}{j\,2\pi s\, z_o}$$

$$\xi = \frac{ms}{\rho_g}$$

$$m = \left|\frac{k\rho_g}{2}\right|^{1/3}$$

$$y_1 = m^{-1}\, kd_1$$

$$y^2 = m^{-1}\, kd_2$$

d_1 = height of source point, P', above cylinder surface

d_2 = height of observation point, P, above cylinder surface

T_o = Torsion Factor = cos δ for a circular cylinder

D = spatial factor = 1 for a circular cylinder

$F_h(\xi, y_1, y_2)$ = "hard" type surface Fock function

$F_s(\xi, y, y_2)$ = "soft" type surface Fock function

p_e = strength of a current moment source at P'

$\mathbf{n}'$ = unit outward normal vector at source point P'

$\hat{\mathbf{n}}$ = unit outward normal vector at observation point P

For $\xi \neq 0$, the Fock function may be approximated by a Taylor series expansion as follows:

$$(3\text{-}2) \quad F_h(\xi, y_1, y_2) = v(\xi) - \frac{j}{4} \xi^{-1} v_1(\xi) [y_1^2 + y_2^2]$$

$$(3\text{-}3) \quad F_s(\xi, y_1, y_2) = u(\xi) + \frac{j}{2} [u'(\xi) - \frac{3}{2} \xi^{-1} u(\xi)] [y_1^2 + y_2^2]$$

According to Pathak and Wang [8], when ξ is large, say $\xi > .6$, a rapidly converging residue series representation for the Fock functions may be utilized as follows:

$$(3\text{-}4) \quad v(\xi) = e^{-j\pi/4} \sqrt{\pi}\, \xi^{1/2} \sum_{n=1}^{\infty} (\tau_n')^{-1} e^{-j\xi\tau_n'}$$

$$(3\text{-}5) \quad u(\xi) = e^{+j\pi/4} 2\sqrt{\pi}\, \xi^{3/2} \sum_{n=1}^{\infty} e^{-j\xi\tau_n}$$

$$(3\text{-}6) \quad v_1(\xi) = e^{j\pi/4} 2\sqrt{\pi}\, \xi^{3/2} \sum_{n=1}^{\infty} e^{-j\xi\tau_n'}$$

$$(3\text{-}7) \quad u'(\xi) = e^{j\pi/4} 3\sqrt{\pi}\, \xi^{1/2} \sum_{n=1}^{\infty} (1 - j\frac{2}{3}\xi\tau_n) e^{-j\xi\tau_n}$$

where τ_n and τ_n' are zeros of the Airy function $w_2(\tau_n)$ and its derivative $w_2'(\tau_n)$, respectively, which are tabulated in Ref. [8] and repeated here for reference in Table 3-1. The Airy function, $w_2(\tau)$, is expressed as:

$$(3\text{-}8) \quad w_2 = \frac{1}{\sqrt{\pi}} \int_{\Gamma_2} dz \exp(\tau z - \frac{z^3}{3})$$

TABLE 3-1

Zeros of $W_2(\tau)$ and $W_2'(\tau)$

$\tau_n = |\tau_n| e^{-j\pi/3}$ and $\tau_n' = |\tau_n'| e^{-i /3}$

n	$\lvert\tau_n\rvert$	$\lvert\tau_n'\rvert$
1	2.33811	1.01879
2	4.08795	3.24819
3	5.52056	4.82010
4	6.78661	6.16331
5	7.94413	7.37218
6	9.02265	8.48849
7	10.0402	9.53545
8	11.0085	10.5277
9	11.9300	11.4751
10	12.8288	12.3848

where integration contour Γ_2 goes from $-\infty$ to 0 along the line arg (z) = $+2\pi/3$ and from 0 to ∞ along the real axis.

If, on the other hand, ξ is a small positive number less than or equal to .6, one may employ a small argument asymptotic expansion for the Fock functions as follows:

$$(3\text{-}9) \quad v(\xi) = 1 - \frac{\sqrt{\pi}}{4} e^{j\pi/4} \xi^{3/2} + j\frac{7}{60}\xi^3 + \frac{7\sqrt{\pi}}{512} e^{j\pi/4} \xi^{4/2} - \ldots$$

$$(3\text{-}10) \quad \mu(\xi) = 1 - \frac{\sqrt{\pi}}{2} e^{j\pi/4} \xi^{3/2} + j\frac{5}{12}\xi^3 + \frac{5\sqrt{\pi}}{64} e^{-j\pi/4} \xi^{9/2} - \ldots$$

$$(3\text{-}11) \quad v_1(\xi) = 1 + \frac{\sqrt{\pi}}{2} e^{j\pi/4} \xi^{3/2} - j\frac{7}{12}\xi^3 - \frac{7\sqrt{\pi}}{64} e^{-j\pi/4} \xi^{9/2} - \ldots$$

$$(3\text{-}12) \quad u'(\xi) = \frac{3}{4}\sqrt{\pi}\, e^{-j3\pi/4} \xi^{1/2} + j\frac{5}{4}\xi^2 + \frac{45}{128}\sqrt{\pi}\, e^{-j\pi/4} \xi^{7/2} - \ldots$$

In the expansion equations, eqns. (3-4) thru (3-7), the first ten terms in the summation may be used. For the small agreement asymptotic expressions, eqns. (3-9) thru (3-12), the first three terms may be used as shown in [8].

At first glance, the mathematics for computing the observed electric field strength may appear to be profuse and overwhelming. However, by confining the convex surface to that of a circular cylinder, the electric field strength of eqn. (3-1) becomes a function of the location of the source and observation points P' and P; the location, orientation, and radius of the circular cylinder; and the magnitude and direction of the current moment at point P', $\bar{p}_e$.

CHAPTER IV

THE HYBRID TECHNIQUE

The hybrid technique seeks to combine the moment method with GTD in an optimum manner so as to yield an analysis procedure for antennas near large electrical bodies which is both efficient and accurate, relying on a minimum number of assumptions.

The basic technique to be described in this paper was first presented in the literature by Thiele and Newhouse [1]. The approach is to first model the wire antennas using the moment method and then modify the generalized impedance matrix to account for the effects of nearby conducting bodies via GTD. This differs from other hybrid approaches which use the moment method to extend GTD [7].

The basic moment method equation, eqn. (2-4),

$$(4\text{-}1) \qquad \int_{-L/2}^{L/2} I(z')K(z_m,z')dz' = -E_z^i(z_m)$$

predicts the electric field strength E_z^i at point z_m which is due to the current function $I(z')$ over a wire of length L. Thru the use of expansion functions, F_n, the wire can be divided into N segments as explained in Chapter II and so that the field at z_m can be written as:

$$(4\text{-}2) \qquad \sum_{n=1}^{N} I_n \int_{\Delta z_n} F_n K(z_m,z_n')dz' = -E_z^i(z_m)$$

Applying a weighting function, W_m, to eqn. (4-2) in order to satisfy the boundary conditions in an average sense over the length of the wire results in

$$(4\text{-}3)\quad \int_{-L/2}^{L/2} W_m \sum_{n=1}^{N} I_n \int_{\Delta z_m} F_n K(z_m,z')dz'dz = \int_{-L/2}^{L/2} W_m \cdot -E_z^i(z_m)dz$$

Interchanging the order of integration and summation

$$(4\text{-}4)\quad \sum_{n=1}^{N} I_n \int_{-L/2}^{L/2} W_m \int_{\Delta z_m} F_n K(z_m,z')dz'dz = \int_{-L/2}^{L/2} W_m \cdot -E_z^i(z_m)dz$$

Following the notation used by Thiele and Newhouse, eqn. (4-4) can be expressed as

$$(4\text{-}5)\quad \sum_{n=1}^{N} I_n \langle W_m, L(J_n)\rangle = \langle W_m, -E_z^i(z_m)\rangle$$

where $L(J_n)$ represents a linear operator which relates the surface expansion currents to the field at point m. Specifically, it can be thought of as the magnitude of the field at point m due to a unit test current at point n. For wires in free space with no other conducting bodies nearby,

$$(4\text{-}6)\quad L(J_n) = \int_{\Delta z_m} F_n K(z_m,z')dz'$$

Referring to eqn. (2-16), eqn. (4-5) can be rewritten as

$$(4\text{-}7)\quad \sum_{n=1}^{N} I_n Z_{mn} = V_m$$

where

(4-8) $Z_{mn} = \langle W_m, L(J_n) \rangle$

(4-9) $V_m = \langle W_m, -E^i_z(z_m) \rangle$

Since the linear operator, L, relates the expansion currents J_n to their electric fields, E, eqn. (4-8) could be expressed as

(4-10) $Z_{mn} = \langle W_m, (\underline{a}E) \rangle$

where $\underline{a}$ is a complex scalar. If conducting bodies are in the vicinity of the wire antennas, eqn. (4-8) can be rewritten as

(4-11) $Z_{mn}' = \langle W_m, L'(J_n) \rangle$

or

(4-12) $Z_{mn}' = \langle W_m, \underline{a}E_1 + \underline{b}E_2 \rangle$

where

E_1 = field arriving at observation point m directly from J_n

E_2 = field arriving at observation point indirectly from J_n due to reflection or diffraction from a conducting body

$\underline{a}$ = complex scalar for E_1

$\underline{b}$ = complex scalar for E_2

Using properties of linear functions,

(4-13) $Z_{mn}' = \langle W_m, aE_1 \rangle + \langle W_m, bE_2 \rangle$

(4-14) $Z_{mn}' = Z_{mn} + Z^g_{mn}$

where

Z_{mn} = the "direct impedance" matrix term which relates the field at segment m that arrives directly, to the current on segment n

Z^{g}_{mn} = the "delta impedance" matrix term which relates the field at segment m that arrives indirectly, due to diffraction or reflection, to the current on segment n

Z_{mn}' = the net impedance matrix term

The hybrid moment method procedure can thus be summarized by the following steps.

1. Completely describe the geometry of the problem; location and size of all wire segments and any conducting bodies in the vicinity.

2. Determine the net impedance matrix terms, Z_{mn}':

   (a) Determine the average field at segment m, if any, which arrives at <u>directly</u> from a test current of one amp at segment n (Z_{mn}).

   (b) Determine the field at segment m, if any, which arrives indirectly, due to reflection by a conducting body, from a test current of one amp at segment n (Z^{r}_{mn}).

   (c) Determine the field at segment m, if any, which arrives indirectly, due to diffraction by a conducting body, from a test current of one amp at segment n (Z^{d}_{mn}).

   (d) For each pair of wire segments n and m, sum the direct and delta impedance matrix terms to obtain the net impedance matrix term for that wire segment pair.

3. Define a field source which will generate an incident, average field, V_m, directly on each segment m. (For transmitting and receiving wire antenna problems, source field [V_m] would be non-zero <u>only</u> for the transmitting antenna segments.)

4. Solve the matrix equation $[I_n] = [Z_{mn}]^{-1} [V_m]$ to obtain the current for every segment of all the wire antennas.

5. Use standard, simple electromagnetic relationships to determine such parameters as the antenna input impedance, radiated power, antenna efficiency, field patterns, mutual coupling between two wire antennas, etc., based on the now known current distribution on the wire antennas.

In order to implement this algorithm in a computer program which would account for cylindrical surface diffraction, the first step was to obtain an efficient moment method program. Richmond's thin wire moment method program [8], incorporates the Galerkin method by using piecewise sinusoidal functions for both the current expansion and the weighting functions. This allows the program to converge using roughly an order of magnitude fewer wire segments than if a pulse basis function point-matching moment method code, solving the same problem, is used. Furthermore, Ekelman had augmented Richmond's code, giving it the capability to deal with reflections from the curved surface of a cylinder as well as diffraction from the sharp edges of a truncated cylinder, by means of using GTD relationships. Therefore, the program was already a hybrid moment method code. In both the basic Richmond code and Ekelman's subroutines, the impedance matrix terms, Z_{mn}, and delta impedance matrix terms, Z^{g}_{mn}, are determined by placing test currents on segment n and determining the resultant field at segment n. The test current distribution (expansion function) is as shown in Fig. 4-1 with n-1 modal currents for each n segment antenna. Thus, a four segment antenna would have three modal currents with the end segments having one modal current each and the other segments each having two modal

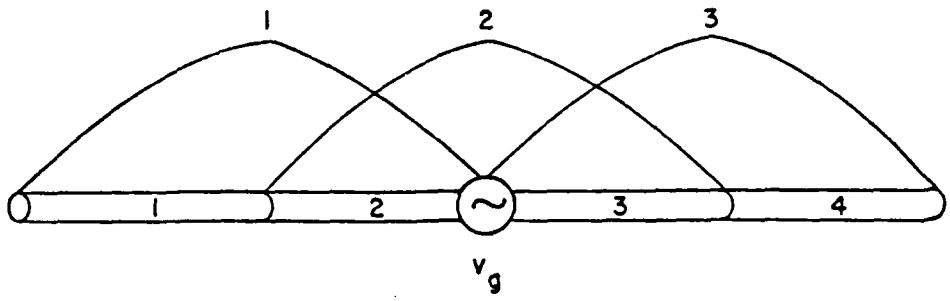

Fig. 4-1. Modal current distribution on a 4 segment wire dipole antenna

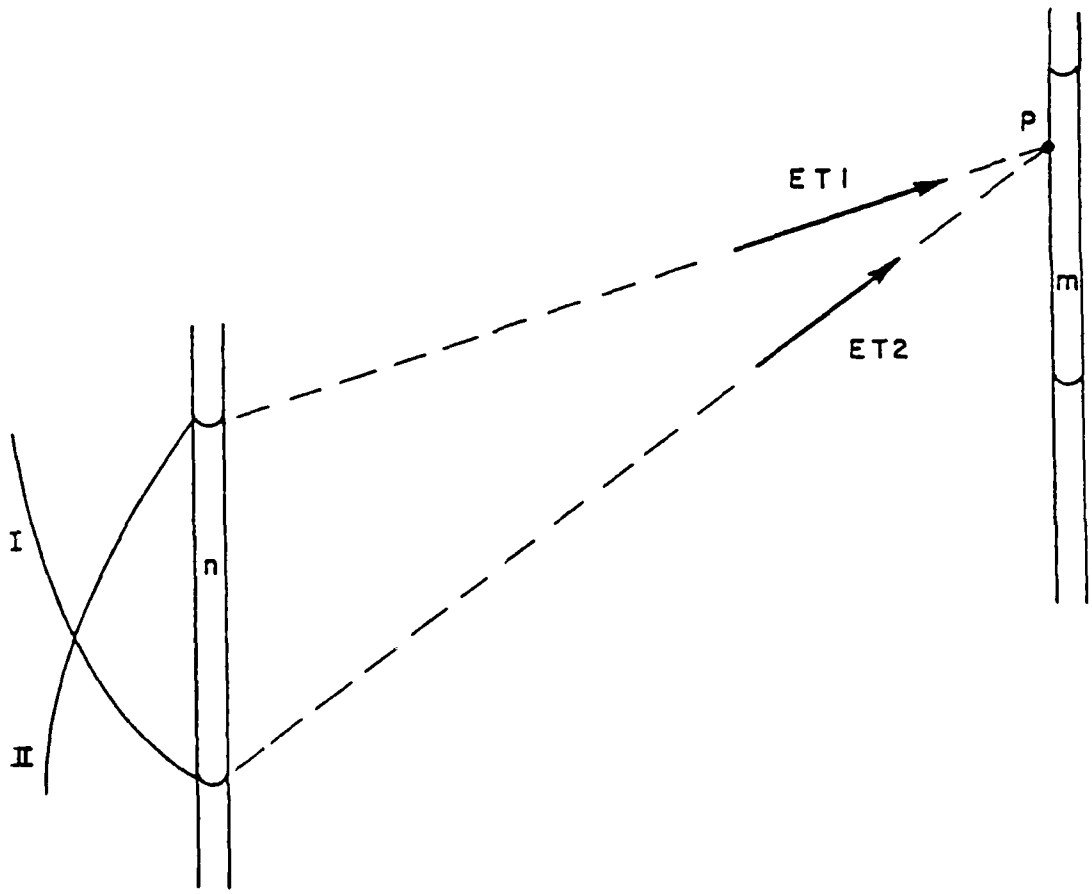

Fig. 4-2. Source and observation segment interaction

currents. The amplitude of each modal current is taken to be one amp. A typical segment n, which is not at either end of the dipole antenna, will therefore contain two modal currents as shown in Fig. 4-2. The program then determines the tangent field observed at various points P which lie on segment m. This field at P is the vector sum of the field contribution from modal current I (ET1) and modal current II (ET2). Numerical integration of the field contributions is performed, resulting in the impedance matrix term or delta impedance matrix term for segments m and n.

For computing the surface diffraction impedance matrix terms, Z_{mn}^{sd}, a test is performed to determine if the surface of the cylinder obstructs the "view" between the test segment n and the observation segment m. If it does not, such as when segments m and n are on the same monopole antenna, the tangential fields are set to zero. Otherwise the tangent field components generated by modal currents I and II on segment n are calculated by subroutines which incorporate the GTD equations as discussed in Chapter III. However, in this case, the modal currents are considered to be located at the midpoint of segment n where the magnitude of each modal current, $\bar{p}_e$, is found as the average value of the current distribution over the wire segment for each modal current. It may be computed in the following manner. As Fig. (4-3) shows, the eight segment antenna is modeled such that nearly one-quarter wavelength of the sinusoidal antenna current is assumed to be distributed over the seven radiating segments. To obtain a more resonant monopole (almost no reactance in the antenna input impedance), the total length of these seven segments was chosen to be .2428 wavelengths. Working in units of radians where one wavelength is equal to 2π radians, the length of the

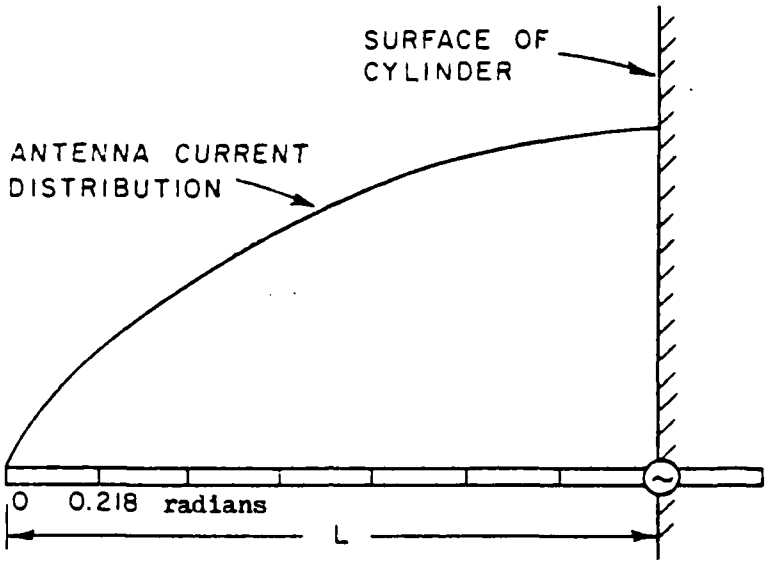

Fig. 4-3. Current distribution on a 1/4 wavelength monopole antenna

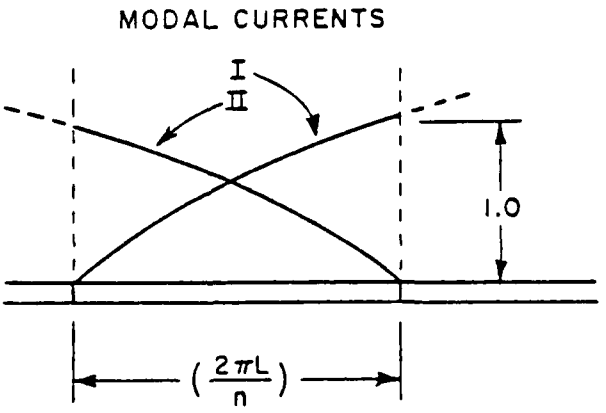

Fig. 4-4. Segment modal current distribution

monopole is equal to 1.526 radians. Therefore, each segment is one-seventh of this length or .2179 radians long on which reside piecewise sinusoidal currents as shown in Fig. 4-4. These segment current distributions are normalized such that their maximum value on the segment is one. In general, the segment current distribution can be described as

$$(4\text{-}15)\quad I(\ell) = \frac{1}{\sin\left(\frac{2\pi L}{n}\right)} \sin \ell$$

where

L = length of the antenna in wavelengths

n = number of radiating equal-length segments in the antenna

By using standard integration techniques, the average value of this current distribution may be determined as follows:

$$(4\text{-}16)\quad I_{av} = \frac{1}{\left(\frac{2\pi L}{n}\right) \sin\left(\frac{2\pi L}{n}\right)} \int_0^{\left(\frac{2\pi L}{n}\right)} \sin \ell \, d\ell$$

Performing the integration yields:

$$(4\text{-}17)\quad I_{av} = \frac{1 - \cos\left(\frac{2\pi L}{n}\right)}{\left(\frac{2\pi L}{n}\right) \sin\left(\frac{2\pi L}{n}\right)}$$

Thus, for $n = 7$ and $L = .2428$, $I_{av} = .502$ amps. This, in turn, is the value that was used for the magnitude of the current moment, $\bar{p}_e$, for the surface diffraction equations. The source and observation segment interaction for surface diffraction is illustrated in Fig. 4-5. The program assumes that the currents on segment n will launch two surface field waves; one which will travel clockwise around the cylinder, the other counterclockwise. Both fields will arrive normal to the surface

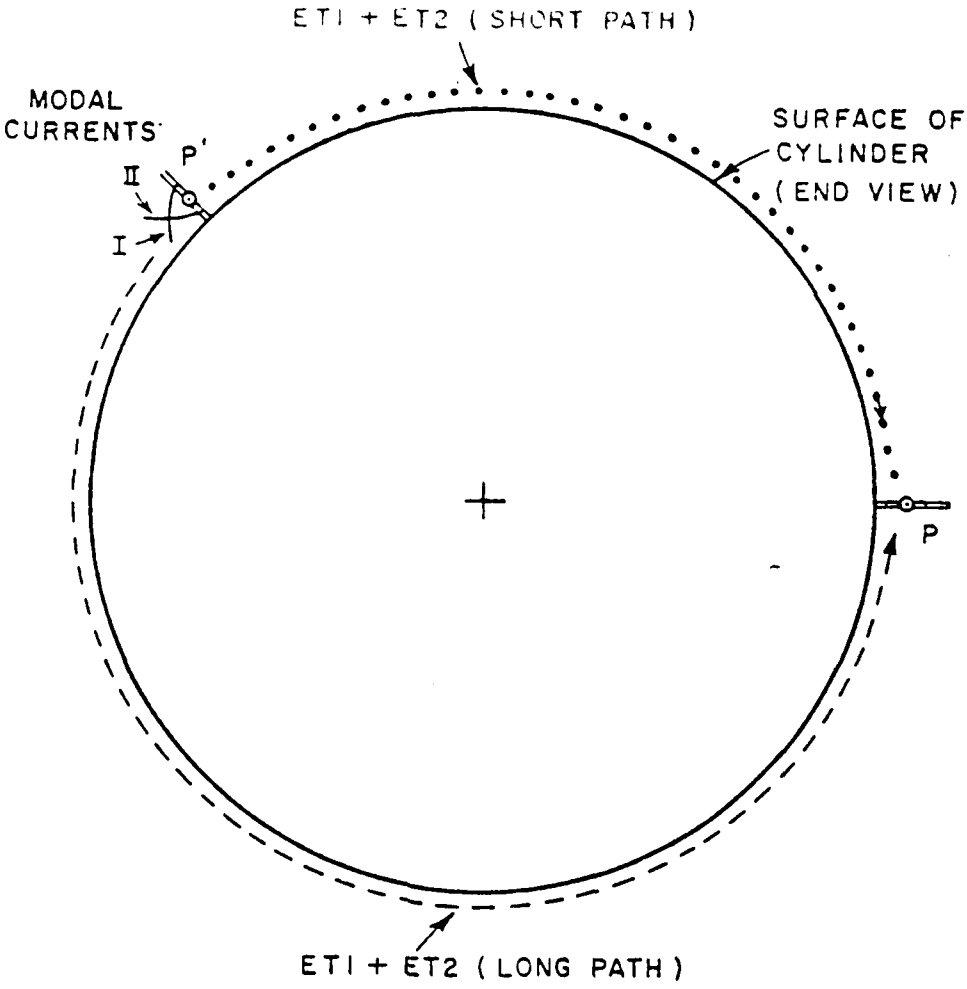

Fig. 4-5. Source and observation point interaction for surface diffraction

of the cylinder at segment m, be added together as vectors, and dotted with the direction of the m^{th} segment on the receiving antenna to yield the total tangential field. As eqn. (3-1) requires, the program also dots the a direction of the source segment modal currents on segment n with the outward normal unit vector of the cylinder. For monopoles normal to the cylinder surface, these dot products are all unity. The tangential fields, ET1 and ET2, are then integrated in the same manner as for the subroutines which determine the impedance matrix terms, Z_{mn}, or reflection delta impedance matrix terms, Z^{r}_{mn}.

CHAPTER V

COMPARISON OF RESULTS WITH AN ALTERNATIVE ANALYSIS PROGRAM

This chapter will discuss an alternative electromagnetic analysis program which is promoted by the United States Air Force (USAF) and will show how well the results of the USAF analysis program agrees with the hybrid method of moments (MOM) program for a variety of cylinder radii and relative antenna locations.

The Intrasystem Electromagnetic Compatibility Analysis Program (IEMCAP) is a USA Standard FORTRAN program for computer-aided implementation of electromagnetic compatibility (EMC) at all stages of an Air Force system's life cycle, applicable to aircraft, space/missile, and ground-based systems [9].

The antenna-to-antenna coupling model, one of the many coupling modes between equipment subsystems which IEMCAP can analyze, is basically a geometric optics (GO) program which determines the severity of interference that a transmitting antenna may unintentionally produce in other antenna receiving systems on the same aircraft due to such phenomena as the generation of higher order harmonics. To use the antenna-to-antenna portion of IEMCAP, one begins by modeling the aircraft as a conducting cylinder with a cone attached at one end. Wings, modeled as infinitely-thin flat plates, can be attached to the

sides of the cylinder. Next, antennas are described by their gain patterns, supplied by the User. Up to three different quantized levels of antenna gain may be specified for the spherical sectors which enclose the antenna. The antennas are then positioned and oriented at their respective locations on the cylinder that represents the aircraft fuselage. The power, frequency range, signal modulation characteristics, and relative harmonic levels of transmitters are enumerated by the User as well as the antennas to which the transmitters are connected. Similarly, the power sensitivity threshold, frequency range, and out-of-band rejection of the receivers, as well as their antennas, are specified by the User. IEMCAP will then determine the magnitude of power delivered to a specific receiving antenna from one of the transmitting antennas, based on the relative position of the antennas on the modeled aircraft, the appropriate gains of the antennas, and the frequency of transmission. The magnitude of the received power is then compared to the receiver's power sensitivity for that frequency and if it exceeds that sensitivity, a potential electromagnetic inference (EMI) problem is predicted by IEMCAP.

In determining the magnitude of the power coupled to the receiving antenna, IEMCAP takes into consideration the distance between the antennas (free-space loss), diffraction around the fuselage (fuselage shading factor), and any diffraction off the edge of the wing which may lie in the direct path between the two antennas (wing diffraction factor). These three factors, all in units of decibels, are added together algebraically with the antenna gains (also in decibels) to arrive at the power coupling factor between the two antennas for a given frequency.

The fuselage shading factor used by IEMCAP is based on work by Hasserjian and Ishimaru [10]. In their analysis, a function is derived which relates the propagation around an infinite conducting cylinder to that over a flat plane. This function is approximated by IEMCAP as follows [11]:

$$(5\text{-}1) \quad SF_c = \frac{-A}{(\eta A + \xi)}$$

where

$$(5\text{-}2) \quad A = \rho_f \, \theta_s^2 \sqrt{\frac{2\pi}{\lambda D_c}}$$

$$\eta = \begin{cases} 5.478 \times 10^{-3} & \text{for } A < 26 \\ 3.340 \times 10^{-3} & \text{for } A \geq 26 \end{cases}$$

$$\xi = \begin{cases} .5083 & \text{for } A < 26 \\ .5621 & \text{for } A \geq 26 \end{cases}$$

and

SF_c = fuselage (cylindrical) shading factor (dB)

ρ_f = radius of cylinder (meters)

θ_s = angle around cylinder of propagation path (radians)

λ = wavelength (meters)

D_c = distance of the cylindrical segment of propagation path

It is possible to compare the performance of the hybrid moment method against that of IEMCAP in computing cylindrical diffraction loss. As part of the standard output, IEMCAP will print the transfer loss between two antennas in units of decibels (dB). This corresponding number can be obtained from the hybrid moment method program in the following manner. The input power to the transmitting antenna can be determined as

(5-3) $P_{in} = \text{Real}\,[V_g I_g^*]$

where

P_{in} = transmitting antenna input power (watts)

V_g = complex voltage at the antenna terminals from a voltage generator (volts)

I_g^* = complex conjugate of the complex current at the antenna terminals (amps)

The power which is received at the other antenna is found by observing the complex current induced in a matched load impedance of 36.2 + j.0104 ohms (input or terminal impedance of a "near" resonant one-quarter wavelength monopole) connected across its terminals and applying the equation

(5-4) $P_{out} = \text{Real}\,[I_r I_r^* Z_L]$

where

P_{out} = power developed at the receiving antenna terminals (watts)

I_r = complex current at the antenna terminals (volts)

I_r^* = complex conjugate current at the antenna terminals (amps)

Z_L = impedance connected across the antenna terminals (ohms) = 36.2 + j.0104

Finally, the transfer loss or power coupling factor may be computed as

(5-5) $PCF = 10.\ \log_{10} \left| \frac{P_{out}}{P_{in}} \right|$

where

PCF = power coupling factor (decibels)

P_{out} = power at receiving antenna (watts)

P_{in} = power input to transmitting antenna

The power coupling factor includes the gain of both the transmitting and receiving antennas. In order to eliminate deviation between the results of the programs due to different values of antenna gains, the effective maximum broadside gain of the monopole modeled by the MOM program was determined in the following manner. A test case was performed in which the transmitting and receiving antennas were located parallel to each other on the surface of a ten wavelength radius cylinder and separated by a distance of exactly ten wavelengths as shown in Fig. 5-1. These wire monopole antennas had a wire radius of .00005 wavelengths and were exactly.2428 wavelengths long. The total power coupling between the transmitting antenna and the receiving antenna was determined by using the procedure previously described and found to be -32.65 dB. Next, the far-field free space loss was computed using the familiar expression:

$$(5\text{-}6) \quad FSL = 10. \log \left| \frac{1}{16\pi^2 D^2} \right|$$

where

FSL = free-space loss (dB)

D = distance between antennas (wavelengths)

Using a value of 10 for D, the value of FSL is approximately -41.98 dB. The difference between these two values is accounted for by the effective gain of each of the two antennas (assumed to be equal). Therefore, the antenna gain is found as

$$(5\text{-}7) \quad Gain = \frac{-32.65 - (-41.98)}{2}$$

or

$$(5\text{-}8) \quad Gain = 4.665 \text{ dB}$$

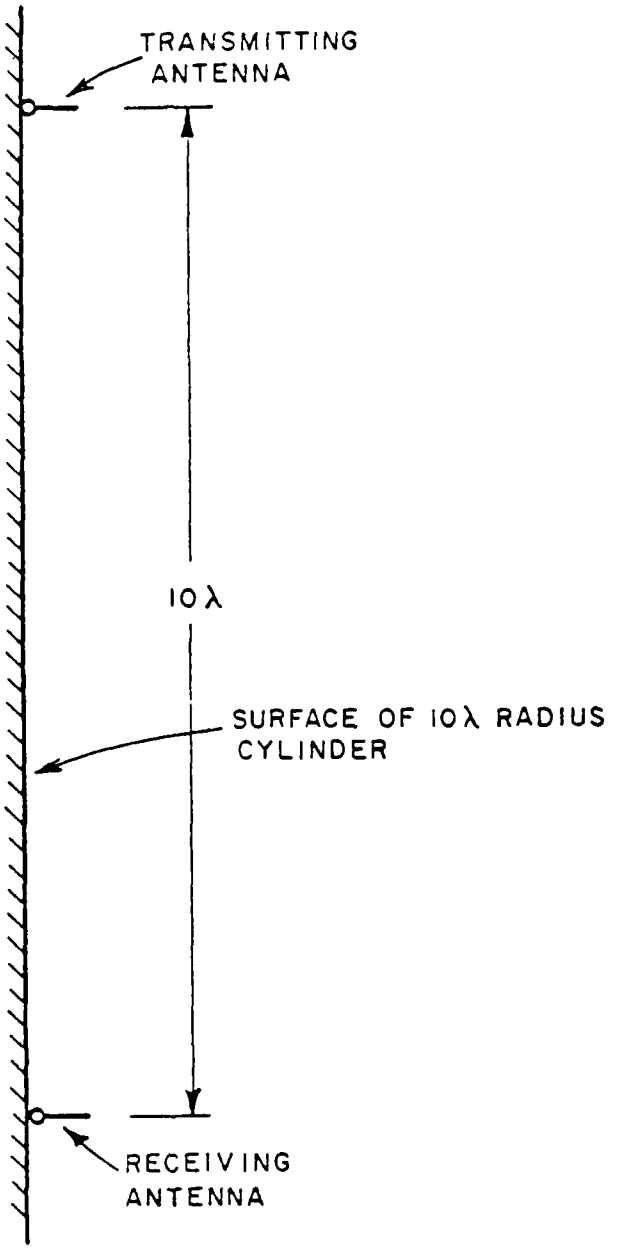

Fig. 5-1. Determination of monopole antenna gain

As a side point, this is very close to the ideal maximum broadside gain of 5.16 dB for a resonant one-quarter wavelength monopole antenna on an infinite flat surface. The gain of 4.665 dB derived by the MOM code for the antenna on a curved surface was used as input data for the IEMCAP code for the one-quarter wavelength monopole antennas.

The next step was to choose an antenna configuration for both programs. For the first configuration, a transmitting monopole antenna was fixed on the surface of a circular cylinder while the receiving monopole antenna was positioned in the plane of the transmitting antenna perpendicular to the cylinder axis, at various angular separations from the transmitting antenna as shown in Fig. 5-2. The radius of the cylinder was initially chosen to be ten wavelengths. This corresponds to the fuselage of a cargo aircraft such as a C-141 or a C-5A at around one gigahertz (GHz), close to the frequencies used by airborne military navigation equipment.

Fig. 5-3 illustrates the excellent agreement between these two radically different approaches for calculating the power coupling factor between two antennas due to cylindrical surface diffraction. Here, values were computed at ten degree intervals. The only significant difference in results between the two methods is when the two antennas are separated by large angles. At these angular separations, both the short and long path diffracted field contributions are similar in magnitude at the receiving antenna. However the difference in the phase angle of the arriving fields results in a reinforcement or cancellation effect. By plotting only the values between 160 and 180 degrees, this phenomenon can be more clearly seen as Fig. 5-4 shows.

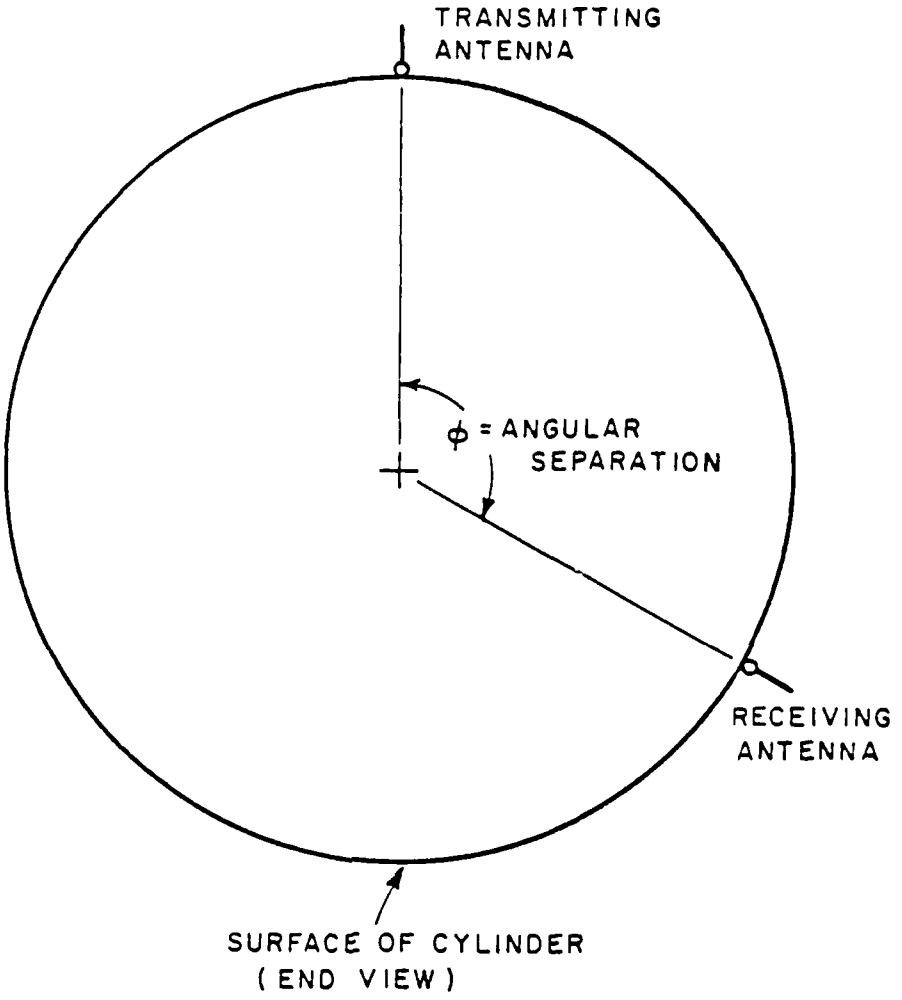

Fig. 5-2. Monopole antennas on a circular cylinder

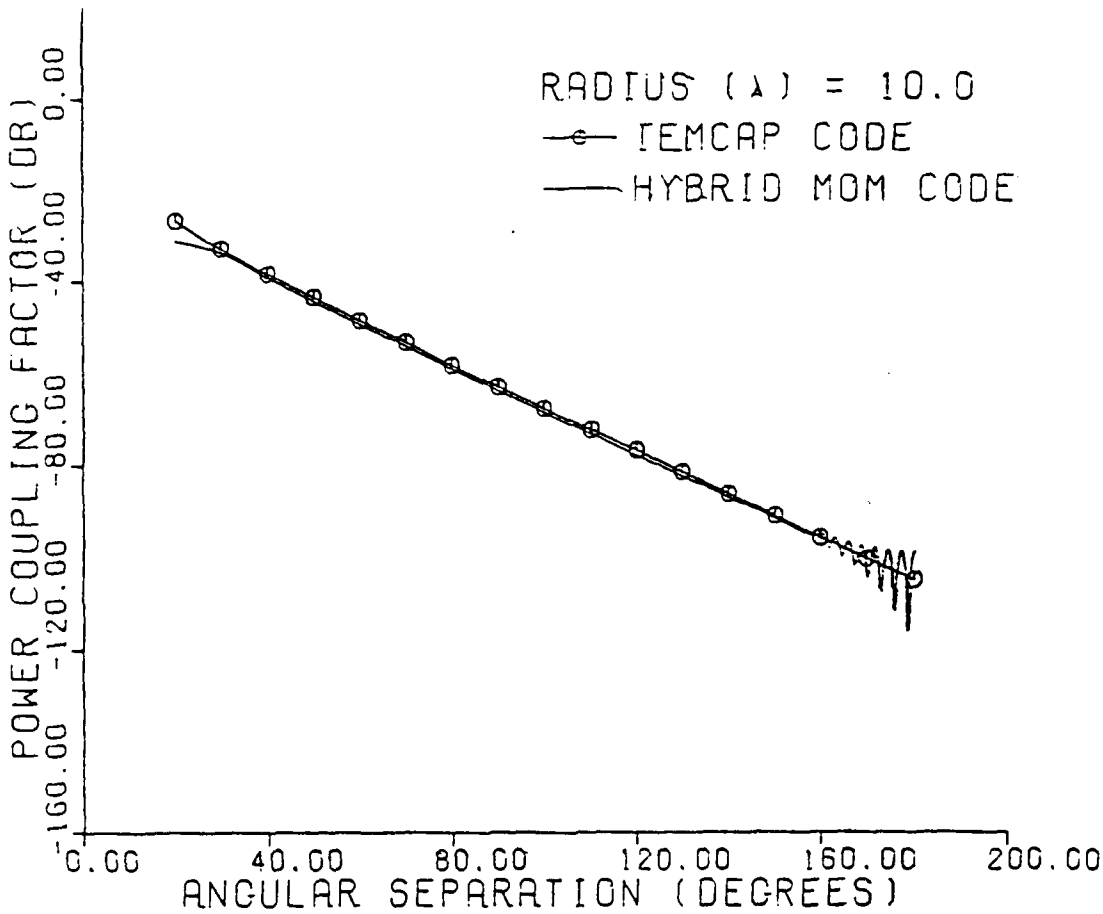

Fig. 5-3. Power coupling factor between two 1/4 wavelength monopoles on a cylinder of radius 10 wavelengths

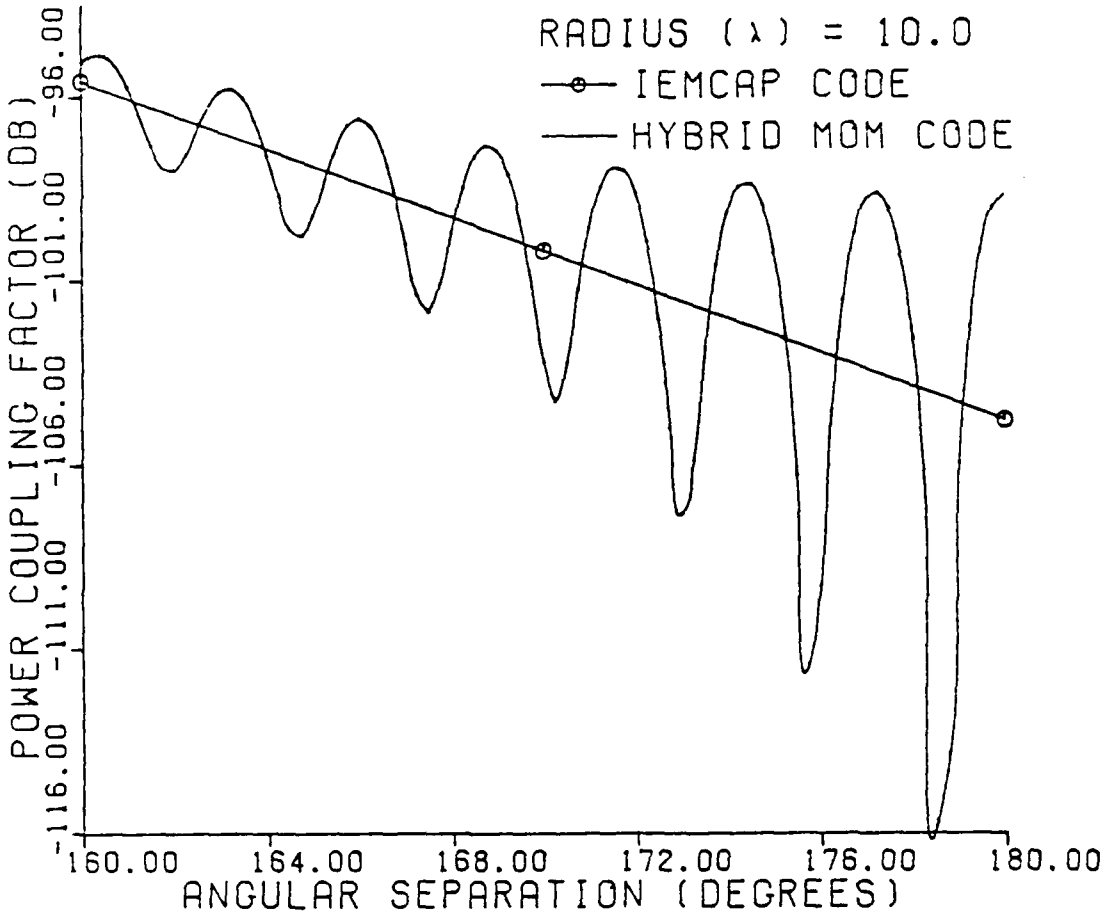

Fig. 5-4. Power coupling factor between two 1/4 wavelength monopoles on a cylinder of radius 10 wavelengths for angular separations between 160 and 180 degrees

The MOM code data in Fig. 5-4 is very similar to a standing wave pattern on a lossy transmission line in the vicinity of a discontinuity. The distance between null points is one-half wavelength. One observes that very close to 180 degrees, the total power received by the second antenna can vary by almost as much as 20 decibels for a displacement of one-quarter wavelength!

Next, the radius of the cylinder was varied. As an upper limit, a cylindrical radius of 150 wavelengths was selected. This corresponds to the fuselage of a C-5A cargo aircraft (30 foot diameter) at a frequency of approximately 10 GHz which is near the operating frequencies of airborne radar, precision approach systems, and electronic warfare (EW) equipment. Fig. 5-5 shows very close agreement between the two approaches for all angular separations less than 130 degrees. As in Fig. 5-3, the MOM data oscillates for angular separations larger than 160 degrees. However, since the separation between the nulls is less than .2 degrees, these oscillations appear as a shaded area.

Figs. 5-6, 5-7, and 5-8 show that the two programs generally yield the same answers for smaller cylinders with a 5, 3, or 1 wavelength radius. Again, there is some deviation for very large angular separations due to the constructive/destructive reinforcement discussed previously. There is also somewhat of a deviation for very small angular separations. This is most likely due to the geometry situation of the antennas and cylinder used by the hybrid MOM code. For these small angles, the electric field is no longer propagating through the surface boundary layer region described in Chapter III. Rather, source points on the transmitting antenna, as well as the observation points

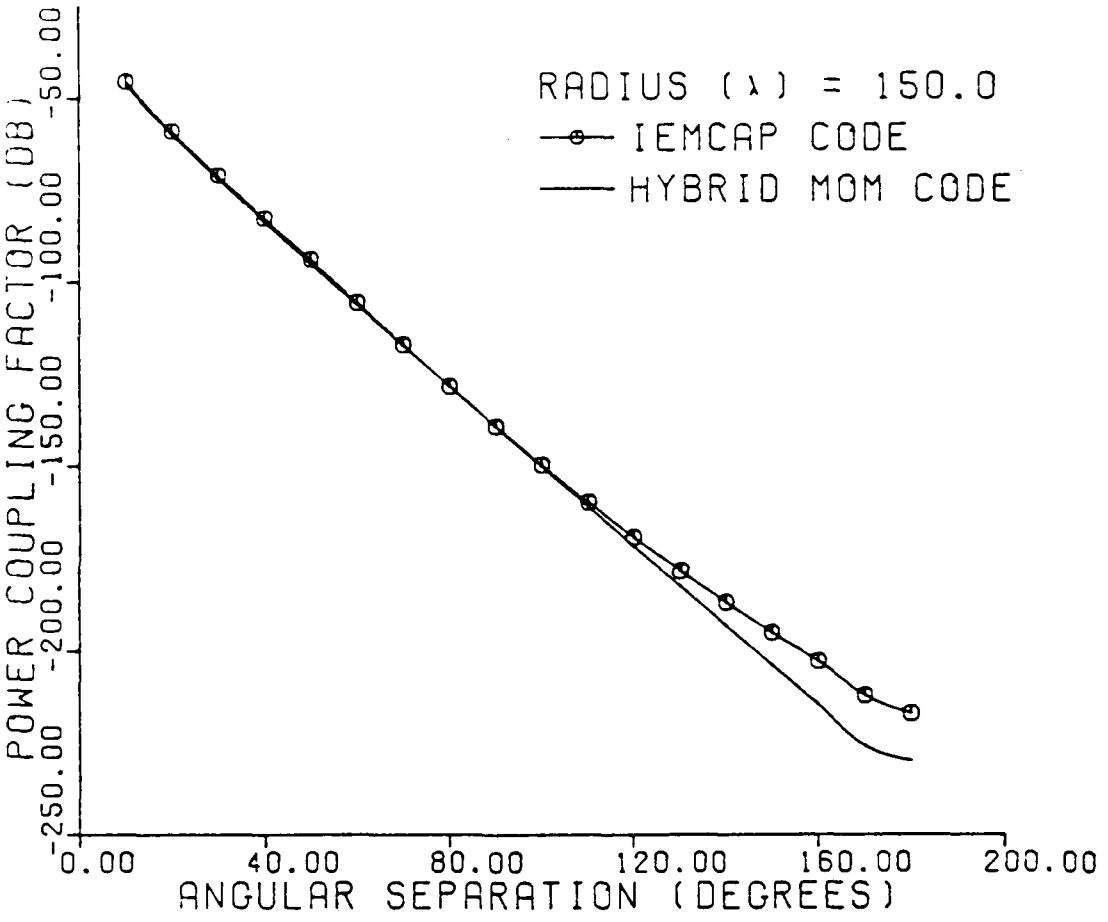

Fig. 5-5. Power coupling factor between two 1/4 wavelength monopoles on a cylinder of radius 150 wavelengths

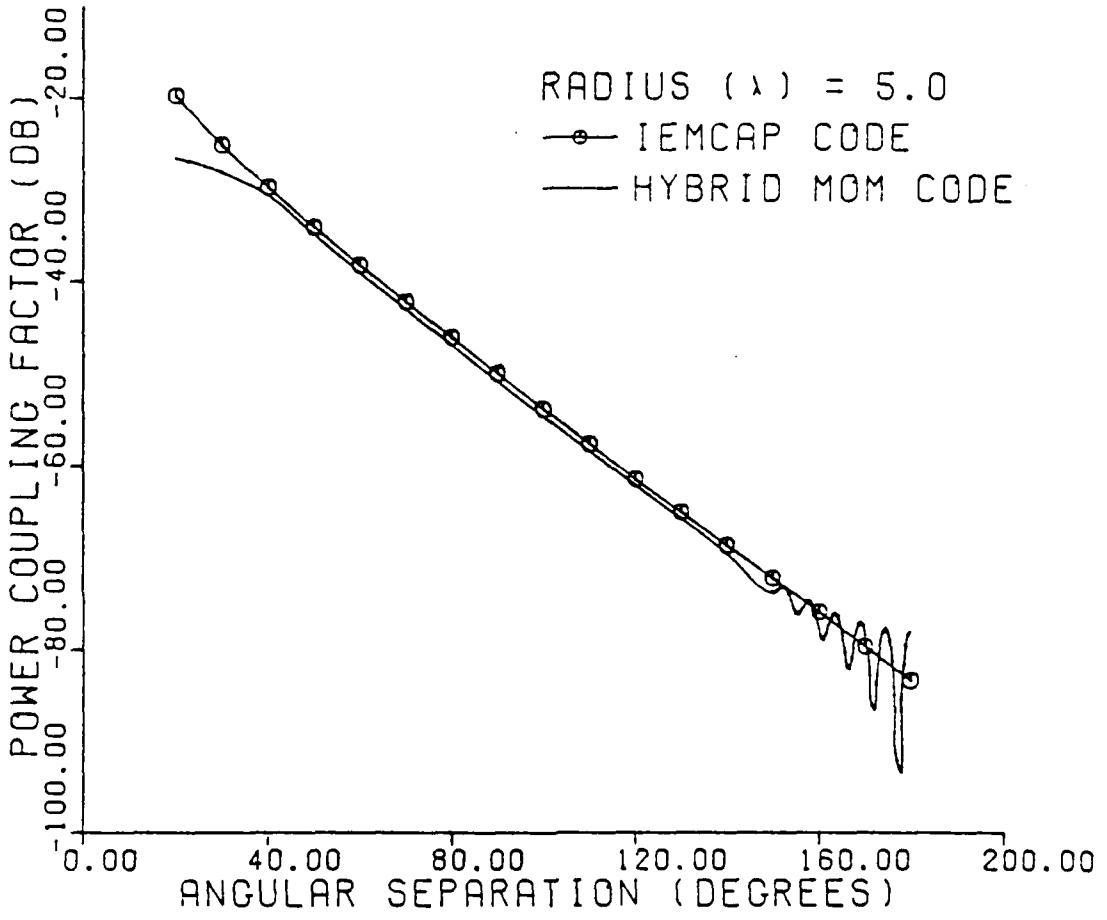

Fig. 5-6. Power coupling factor between 1/4 wavelength monopoles on a cylinder of radius 5 wavelengths

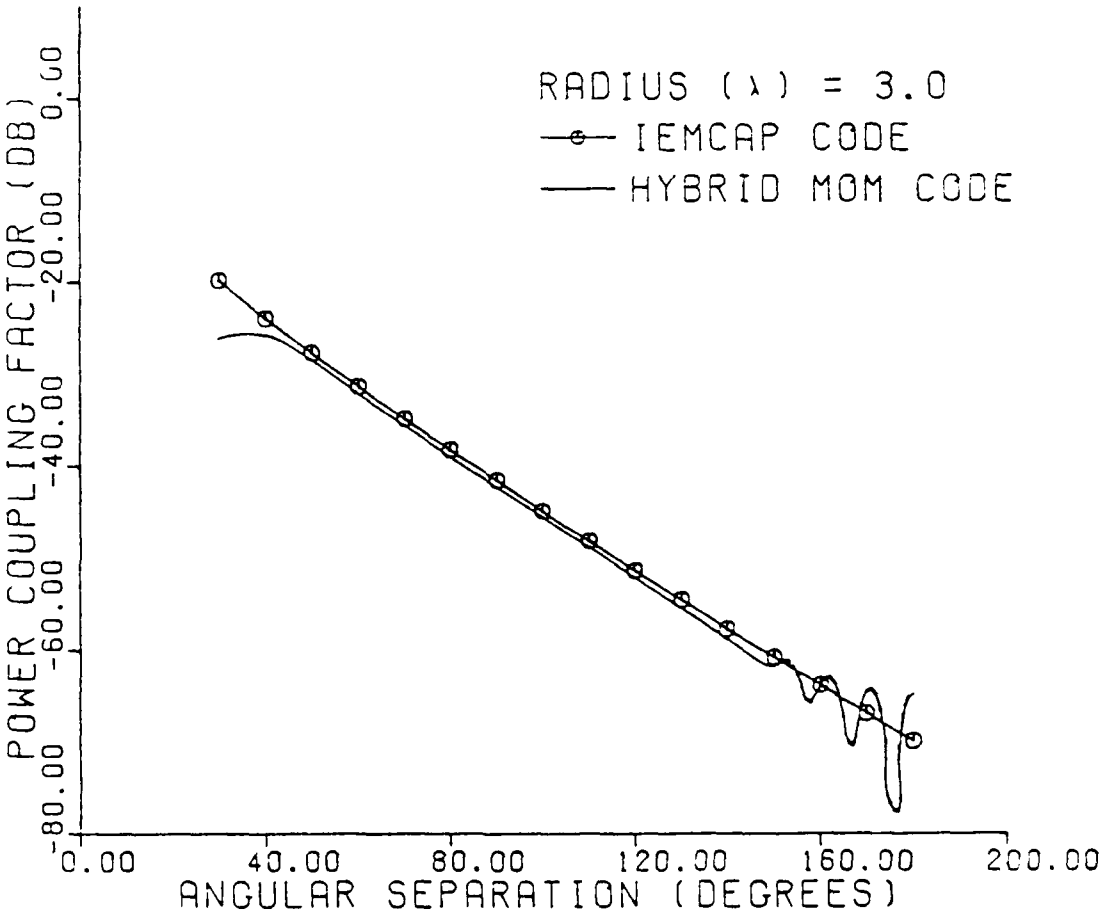

Fig. 5-7. Power coupling factor between two 1/4 wavelength monopoles on a cylinder of radius 3 wavelengths

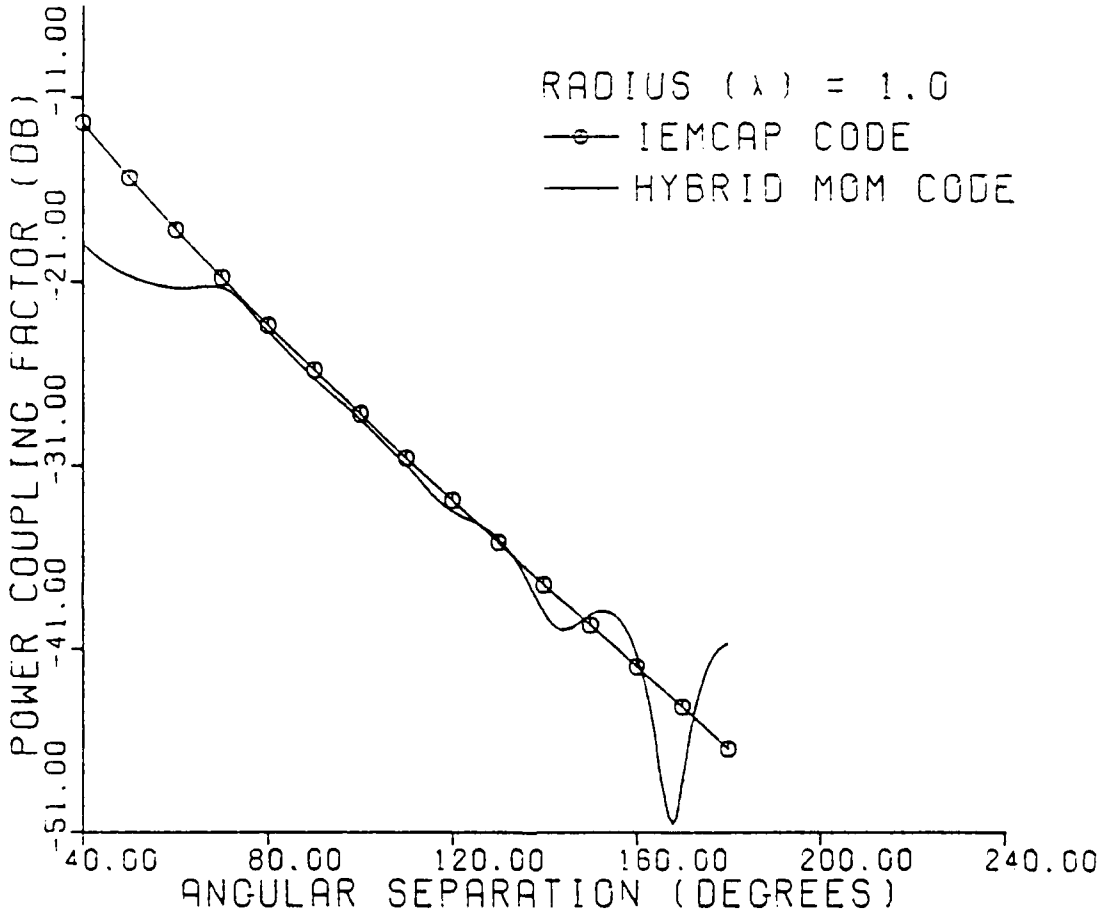

Fig. 5-8. Power coupling factor between two 1/4 wavelength monopoles on a cylinder of radius 1 wavelength

on the receiving antenna, may more properly be considered as points well off the cylinder surface, especially for the antenna segments farthest away from the cylinder surface. Therefore, a different set of surface diffraction equations should be used which permits the source and/or observation point to be outside the surface boundary layer [6].

A case which lends additional support to this deduction is that of the five-eigths wavelength monopole. The length of the one-quarter wavelength monopole was extended to .625 wavelengths. The matched load impedance was now found to be 73.5 + j400.7 ohms. The antenna effective gains were computed by the MOM code as before and found to be 8.385 dB, nearly equal to the ideal maximum broadside gain of 8.7 dB. This value of 8.385 dB was used as the gain of the antennas in the IEMCAP code. Fig. 5-9 illustrates the results of the two programs. Here the deviation between the two codes is becoming significant. With the antennas more than one-quarter wavelength above the cylinder surface, many more source and reception points on the antennas are no longer in the surface boundary layer region. Thus, as for one-quarter wavelength monopoles on smaller radii cylinders, the MOM code appears to be less accurate.

A second type of orientation of the antennas on the fuselage was used to introduce torsion in the paths between the antennas. The antennas now are no longer in the same plane perpendicular to the cylinder axis as before. They are separated by both an angular displacement as well as a displacement along the cylinder axis which lies on the z axis.

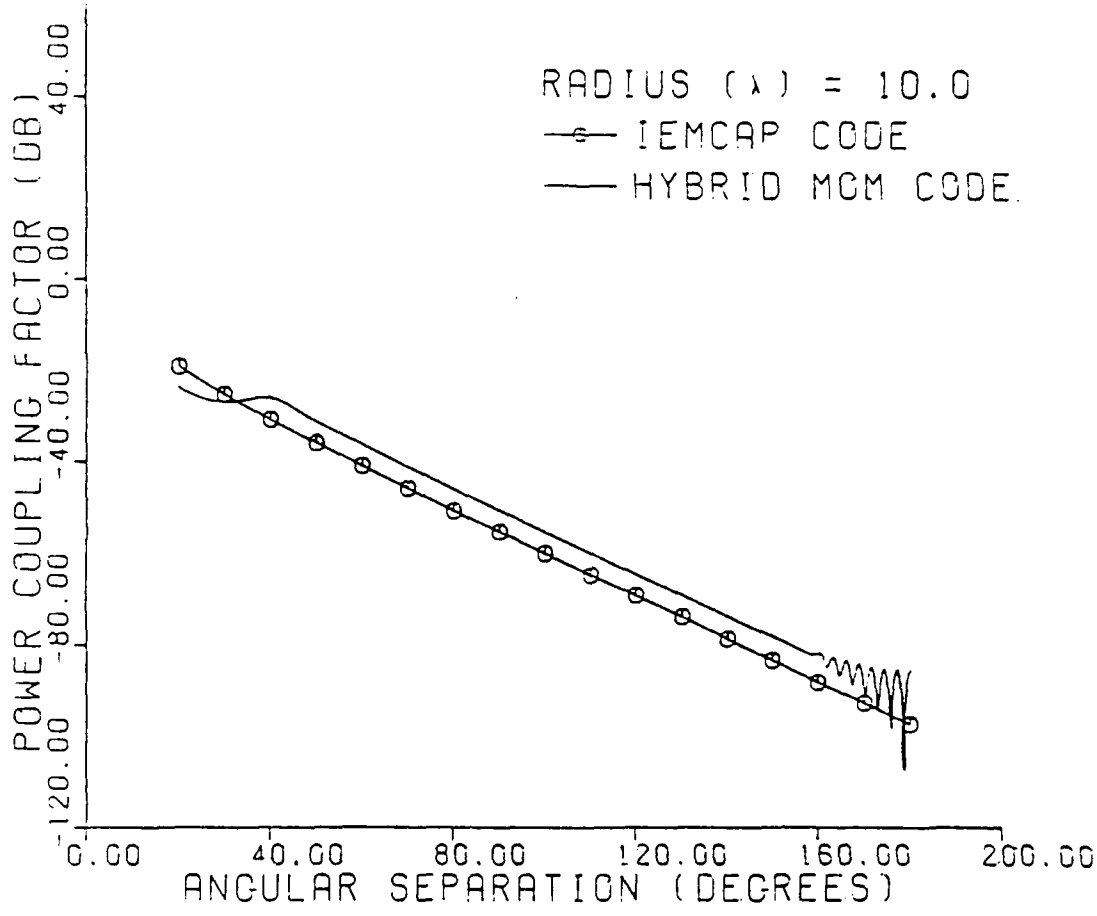

Fig. 5-9. Power coupling factor between two 5/8 wavelength monopoles on a cylinder of radius 10 wavelengths

Specifically, two cases of constant angular displacements of 90 and 180 degrees were chosen where the power coupling factor was computed and plotted as a function of linear separation parallel to the cylinder axis. These orientations are illustrated in Fig. 5-10.

The results of the power coupling factors computed by both the MOM code and the IEMCAP code for angular separations of 90 degrees is graphed in Fig. 5-11. The agreement between these two methods is amazingly close for all four linear separations computed.

Fig. 5-12 compares the results of the IEMCAP to the MOM code when the angular separation is 180 degrees. Although the two codes produce answers that differ by approximately 6 dB, this difference is most likely due to phase information that the MOM code accounts for which the IEMCAP code does not (as explained in detail previously in this chapter). However, both codes predict nearly equal changes in the power coupling factor for corresponding changes in linear displacement along the cylinder axis. Furthermore, for the 180 degree angular displacement case, both codes show that the power coupling factor will actually increase as linear displacement between the two antennas is increased.

Based on these comparisons between the MOM code and the IEMCAP code in their ability to determine the loss in transmitted power due to cylindrical surface diffraction, several conclusions may be drawn. For intermediate angular separations (60 to 120 degrees), the deviation in results between the two codes is less than one decibel. This is a strong indication that both results are correct. For larger angular separations (120° to 180°) deviation between the codes can be explained by the reinforcement/cancellation effects due to phase information which is accounted for by the MOM code but not by IEMCAP. Yet the IEMCAP code

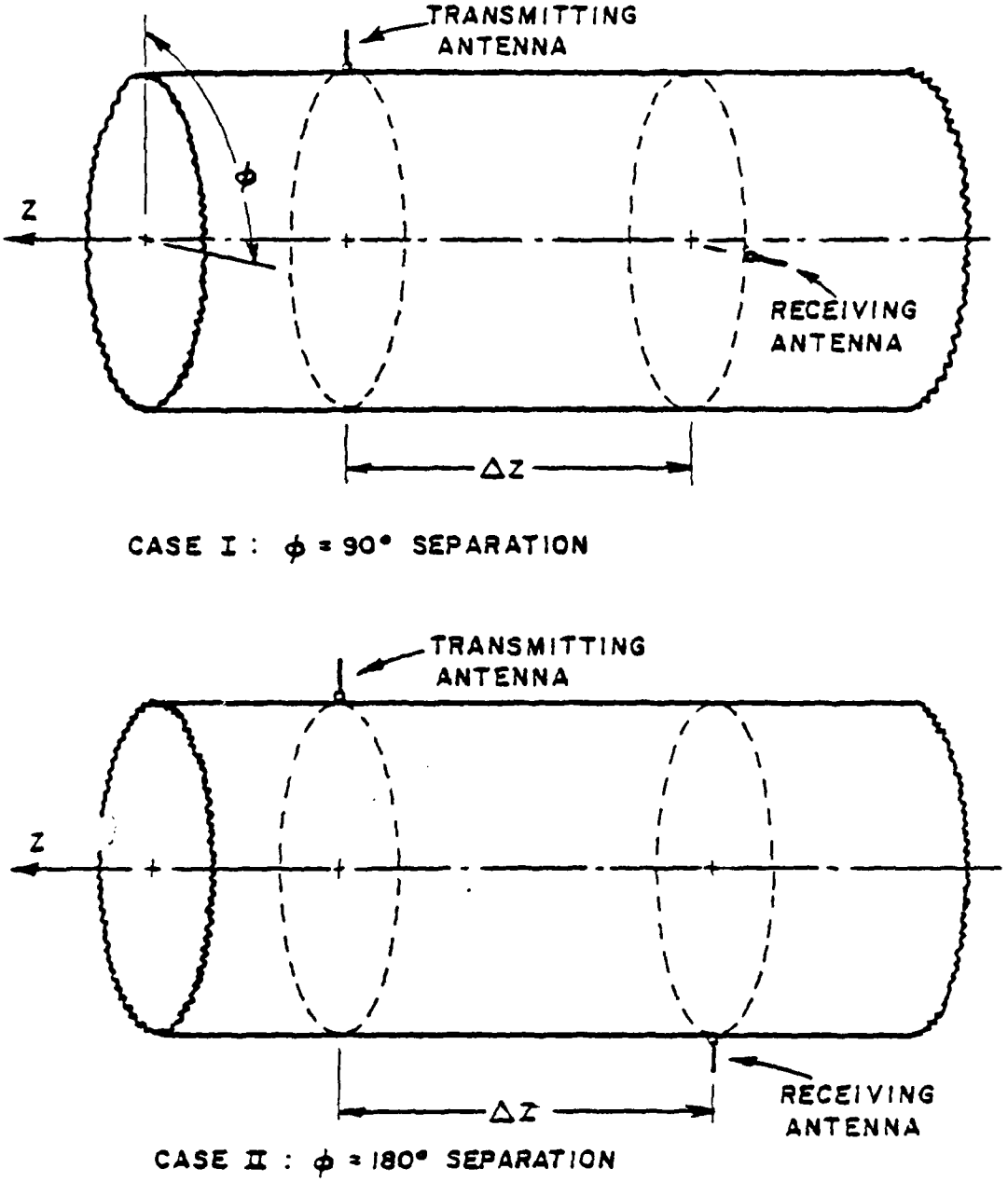

Fig. 5-10. Coupling paths with torsion

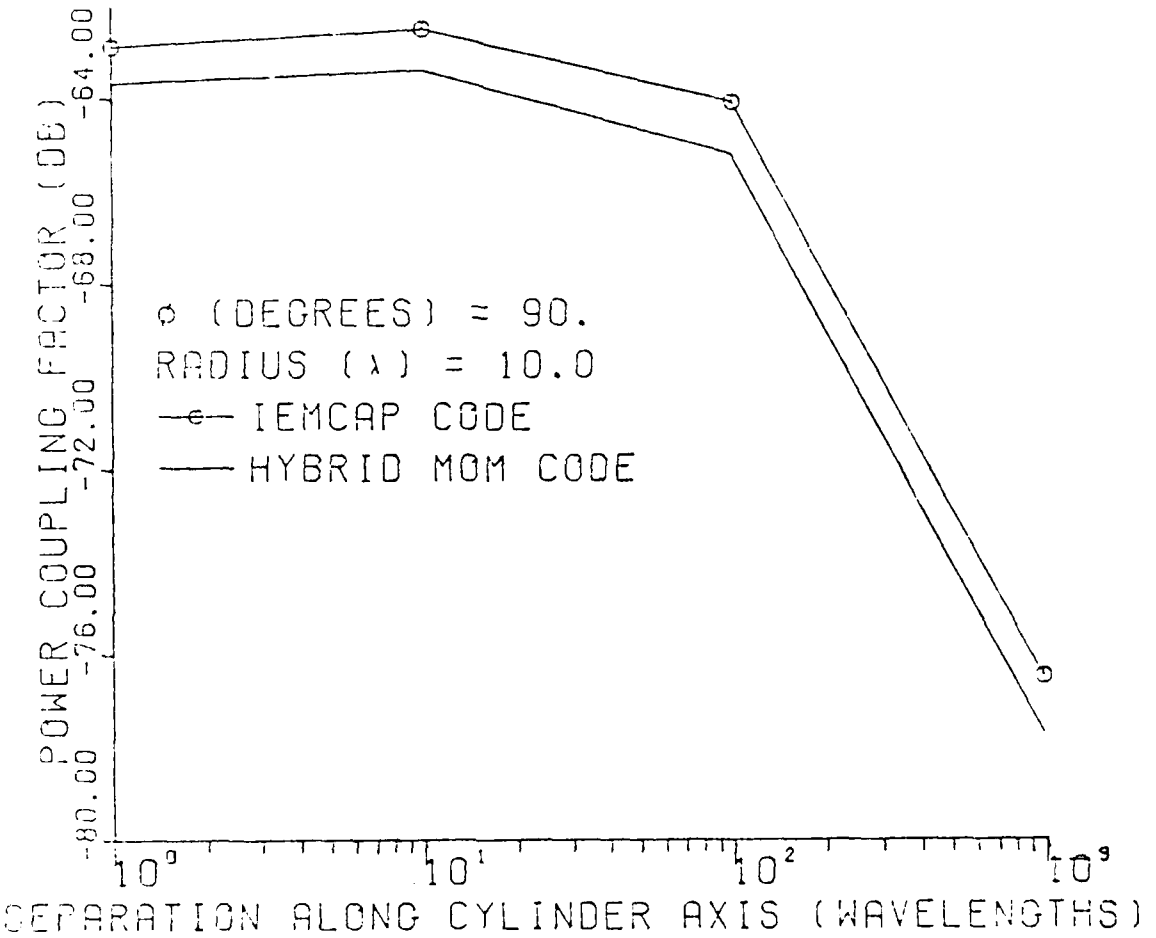

Fig. 5-11. Power coupling factor between two 1/4 wavelength monopoles on a cylinder of radius 10 wavelengths, at a constant angular separation of 90 degrees

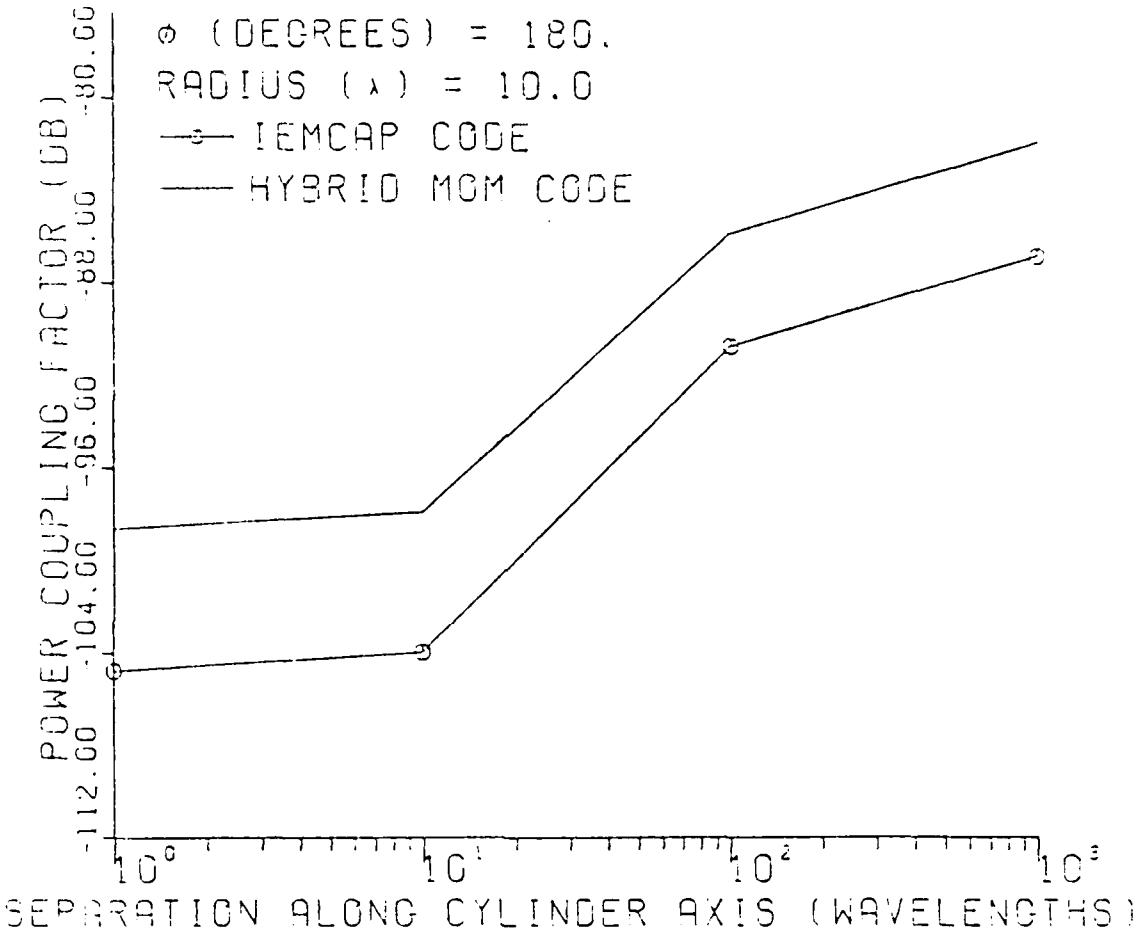

Fig. 5-12. Power coupling factor between two 1/4 wavelength monopoles on a cylinder of radius 10 wavelengths at a constant angular separation of 180 degrees

values do agree with the average values of the standing-wave type patterns of the MOM code results. Thus, the MOM code results appear to be correct for cylindrical surface diffraction involving large angles. In addition, there is also good agreement between the two codes for cases of linear displacement along the axis of the cylinder where torsion is introduced into the path between the transmitting and receiving antennas.

However, deviation between results of the two codes is more severe for small angular separations (less than 60 degrees) between one-quarter wavelength monopoles on small cylinders with radii on the order of one wavelength. There is also a disturbing amount of disparity between the results of the MOM and IEMCAP codes when a longer five-eights wavelength monopole is used. It appears that the MOM code fails (gracefully) when source points are much more than one-quarter wavelength above the cylinder surface or when very little of the propagation path between the antennas resides in the surface boundary region, as for small angular separations on small radii cylinders. To reduce the effect of these problems, equations which account for curved surface diffraction from source and observation points outside the surface boundary layer, such as described by Pathak, Burnside, and Marhefka [6], should be considered.

APPENDIX A

DESCRIPTION OF SUBROUTINES

The purpose of this appendix is to furnish a brief description of the subroutines which were added to Richmond's thin-wire program in order to account for surface wave diffraction around a circular cylinder. For a description of the subroutines used in the original thin-wire program or the subroutines developed by Ekelman which account for reflection from the surface of the cylinder, the reader is advised to consult References [3] or [2] respectively.

Subroutine SGANTC, listed in Fig. A-1, is called in place of SGANT. Subroutine SGANTC is the same as subroutine SGANT, described in Reference [3], with two exceptions. First of all, subroutine GGSCYL is called instead of GGS. Secondly, the statements which modify the mutual impedance matrix C to account for lumped impedances contained in the ZLD matrix, have been modified to accommodate the C matrix, stored as a two-dimension array instead of the original single-dimension array used in Richmond's program.

Subroutine GGSCYL, listed in Fig. A-2, is similar to subroutine GGS, of the original thin-wire program, described in Reference [3]. However, GGSCYL will test if the surface of the cylinder obstructs the line of sight between the end points of the source and observation segments. This is done by calling subroutine VISIBLE whose parameters

```
      SUBROUTINE SGANTC(ICJ,IA,IB,INM,INT,ISC,I1,I2,I3,JA,JB,MD,N,ND,NM,
     2  NP,AM,BM,C,CGD,CMM,D,EP2,EP3,ETA,FHZ,GAM,SGD,
     3  X,Y,Z,ZLD,ZS,I2NM,RADM)
C * * SGANTC IS THE SAME AS SGANT EXCEPT THAT GGSCYL IS CALLED INSTEAD
C * * OF GGS.
      COMPLEX ZG,ZH,ZS,EGD,GD,CGDS,SGDS,SGDT,B01
      COMPLEX P11,P12,P21,P22,Q11,Q12,Q21,Q22,EP2,EP,ETA,GAM,EP3
      COMPLEX EPSILA,CWEA,BETA,ZARG
      COMPLEX P(2,2),Q(2,2),CGD(INM),SGD(INM),C(ICJ,ICJ),ZLD(I2NM)
      DIMENSION X(NP),Y(NP),Z(NP),D(INM),IA(INM),IB(INM),MD(INM,4)
      DIMENSION I1(ICJ),I2(ICJ),I3(ICJ),JA(ICJ),JB(ICJ),ND(INM),ISC(INM)
      DATA E0,TP,U0/8.854E-12,6.28318,1.2566E-6/


    2 FORMAT(3X,*AM = *,E10.3,3X,*DMAX = *,E10.3,3X,*DMIN = *,E10.3)
      EP=EP3
      ICC=(N*N+N)/2
      DO 11 J=1,N
      DO 10 I=1,N
   10 C(I,J)=(0.,0.)
   11 CONTINUE
      ZS=(.0,.0)
      IF(CMM.LE.0.)GO TO 12
      OMEGA=TP*FHZ
      EPSILA=CMPLX(E0,-CMM*1.E6/OMEGA)
      CWEA=(.0,1.)*OMEGA*EPSILA
      BETA=OMEGA*SQRT(U0)*CSQRT(EPSILA-EP)
      ZARG=BETA*AM
      CALL CBES(ZARG,B01)
      ZS=BETA*B01/CWEA
   12 ZH=ZS/(TP*AM*GAM)
      DMIN=1.E30
      DMAX=.0
      DO 20 J=1,NM
      K=IA(J)
      L=IB(J)
      D(J)=SQRT((X(K)-X(L))**2+(Y(K)-Y(L))**2+(Z(K)-Z(L))**2)
      IF(D(J).LT.DMIN)DMIN=D(J)
      IF(D(J).GT.DMAX)DMAX=D(J)
      EGD=CEXP(GAM*D(J))
      CGD(J)=(EGD+1./EGD)/2.
   20 SGD(J)=(EGD-1./EGD)/2.
      IF(DMIN.LT.2.*AM)GO TO 25
      IF(CABS(GAM*AM).GT.0.06)GO TO 25
      IF(CABS(GAM*DMAX).GT.3.)GO TO 25
      IF(AM.GT.0.)GO TO 30
   25 N=0
      WRITE(6,2)AM,DMAX,DMIN
      RETURN
   30 DO 200 K=1,NM
      NDK=ND(K)
      KA=IA(K)
      KB=IB(K)
      DK=D(K)
      CGDS=CGD(K)
      SGDS=SGD(K)
      DO 200 L=1,NM
      NDL=ND(L)
      LA=IA(L)
      LB=IB(L)
      DL=D(L)
      SGDT=SGD(L)
      NII=0
      DO 200 II=1,NDK
```

Fig. A-1. Subroutine SGANTC

```
      I=MD(F,II)
      MM=(I-1)*N-(I*I-I)/2
      FI=1.
      IF(KB.EQ.I2(I))GO TO 36
      IF(KB.EQ.I1(I))FI=-1.
      IS=1
      GO TO 40
   36 IF(KA.EQ.I3(I))FI=-1.
      IS=2
   40 DO 200 JJ=1,NDL
      J=MD(L,JJ)
      MMM=MM+J
      IF(I.GT.J)GO TO 200
      FJ=1.



      IF(LB.EQ.I2(J))GO TO 46
      IF(LB.EQ.I1(J))FJ=-1.
      JS=1
      GO TO 50
   46 IF(LA.EQ.I3(J))FJ=-1.
      JS=2
   50 IF(NIL.NE.0)GO TO 168
      NIL=1
      IF(K.EQ.L)GO TO 120
      IND=(LA-KA)*(LB-KA)*(LA-KB)*(LB-KB)
      IF(IND.EQ.0)GO TO 80
C     SEGMENTS K AND L SHARE NO POINTS
      CALL GGSCYL(X(KA),Y(KA),Z(KA),X(KB),Y(KB),Z(KB),X(LA),Y(LA),Z(LA),
     2  X(LB),Y(LB),Z(LB),RADM,AM,DK,CGDS,SGDS,DL,SGDT,INT,ETA,GAM
     3,P(1,1),P(1,2),P(2,1),P(2,2))
      GO TO 168
C     SEGMENTS K AND L SHARE ONE POINT (THEY INTERSECT)
   80 KG=0
      JM=KB
      JC=KA
      KF=1
      IND=(KB-LA)*(KB-LB)
      IF(IND.NE.0)GO TO 82
      JC=KB
      KF=-1
      JM=KA
      KG=3
   82 LG=3
      JP=LA
      LF=-1
      IF(LB.EQ.JC)GO TO 83
      JP=LB
      LF=1
      LG=0
   83 SGN=KF*LF
      CPSI=((X(JP)-X(JC))*(X(JM)-X(JC))+(Y(JP)-Y(JC))*(Y(JM)-Y(JC))
     2+(Z(JP)-Z(JC))*(Z(JM)-Z(JC)))/(DK*DL)
      CALL GGMM(.0,DK,.0,DL,AM,CGDS,SGDS,SGDT,CPSI,ETA,GAM
     2,Q(1,1),Q(1,2),Q(2,1),Q(2,2))
      DO 98 KK=1,2
      KP=IABS(KK-KG)
      DO 98 LL=1,2
      LP=IABS(LL-LG)
      P(KP,LP)=SGN*Q(KK,LL)
   98 CONTINUE
      GO TO 168
C     K=L  (SELF REACTION OF SEGMENT K)
  120 Q11=(.0,.0)
```

Fig. A-1. (Continued)

```
      Q12=(.Ø,.Ø)
      IF(CMM.LE.Ø.)GO TO 15Ø
      GD=GAM*DK
      ZG=ZH/(SGDS**2)
      Q11=ZG*(SGDS*CGDS-GD)/2.
      ZG=ZH/(SGDS**2)
      Q11=ZG*(SGDS*CGDS-GD)/2.
      Q12=ZG*(GD*CGDS-SGDS)/2.
  15Ø ISCK=ISC(K)
      P11=(.Ø,.Ø)
      P12=(.Ø,.Ø)
      IF(ISCK.EQ.Ø)GO TO 155
      IF(BM.LE.AM)GO TO 155
      CALL        DSHELL(AM,BM,DK,CGDS,SGDS,EP2,EP,ETA,GAM,P11,P12)
  155 Q11=P11+Q11
      Q12=P12+Q12



      CALL GGMM(.Ø,DK,.Ø,DK,AM,CGDS,SGDS,SGDS,1.
     2.ETA,GAM,P11,P12,P21,P22)
      Q11=P11+Q11
      Q12=P12+Q12
      P(1,1)=Q11
      P(1,2)=Q12
      P(2,1)=Q12
      P(2,2)=Q11
      IF(KA.NE.LA)GO TO 16Ø
      GO TO 168
  16Ø P(1,1)=-Q12
      P(1,2)=-Q11
      P(2,1)=-Q11
      P(2,2)=-Q12
  168 C(I,J)=C(I,J)+FI*FJ*P(IS,JS)
      IF(I.NE.J)C(J,I)=C(I,J)
  2ØØ CONTINUE
C  ADD THE LUMPED IMPEDANCES TO THE C MATRIX.
      ISEG=1
  3Ø1 IF(ZLD(ISEG).NE.(Ø.,Ø.)) GO TO 3Ø2
      IF(ISEG.EQ.I2NM) GO TO 35Ø
  3Ø3 ISEG=ISEG + 1
      GO TO 3Ø1
  3Ø2 IMODE=1
  3Ø7 IF(ISEG.GT.INM) GO TO 3Ø4
      IF(I2(IMODE).EQ.IA(ISEG)) GO TO 3Ø5
  3Ø6 IMODE=IMODE + 1
      IF(IMODE.GT.N) GO TO 36Ø
      GO TO 3Ø7
  3Ø4 ISEG=ISEG - INM
      IF(I2(IMODE).EQ.IB(ISEG)) GO TO 3Ø5
      ISEG=ISEG + INM
      GO TO 3Ø6
  3Ø5 C(IMODE,IMODE)=C(IMODE,IMODE) + ZLD(ISEG)
      GO TO 3Ø3
  35Ø CONTINUE
      RETURN
  36Ø WRITE(6,6Ø1) ISEG,ZLD(ISEG)
  6Ø1 FORMAT(1X,*FATAL ERROR:  UNABLE TO FIND DIPOLE MODE TERMINALS*/
     1  * FOR LUMPED IMPEDANCE ZLD(*,I3,*) = *,2E15.6)
      N=-1
      GO TO 35Ø
      END
```

Fig. A-1. (Continued)

```
      SUBROUTINE GGSCYL(XA,YA,ZA,XB,YB,ZB,X1,Y1,Z1,X2,Y2,Z2,RADM,AM
     2,DS,CGDS,SGDS,DT,SGDT,INT,ETA,GAM,P11,P12,P21,P22)
      COMPLEX P11,P12,P21,P22,EJA,EJB,EJ1,EJ2,ETA,GAM,C1,C2,CST
      COMPLEX EGD,CGDS,SGDS,SGDT,ER1,ER2,ET1,ET2
      COMPLEX ER11,ER12,ER21,ER22
      COMPLEX ET11,ET12,ET21,ET22
      LOGICAL AVIS,BVIS,VIS
      DATA FP/12.56637/
      CA=(X2-X1)/DT
      CB=(Y2-Y1)/DT
      CG=(Z2-Z1)/DT
      CAS=(XB-XA)/DS
      CBS=(YB-YA)/DS
      CGS=(ZB-ZA)/DS
      CC=CA*CAS+CB*CBS+CG*CGS
      IF(ABS(CC).GT..597)GO TO 200
   20 SZ=((1-XA)*CAS+(Y1-YA)*CBS+(Z1-ZA)*CGS
C
C   THIS VERSION OF GGS WILL TEST IF CYLINDER SURFACE
C   PREVENTS "VISIBILITY" BETWEEN THE TWO SEGENTS.
C
      IF(INT.GT.0) GO TO 301
      CALL VISIBLE(XA,YA,X1,Y1,RADM,VIS)
      IF(.NOT.VIS) GO TO 301
      CALL VISIBLE(XB,YB,X2,Y2,RADM,VIS)
      IF(.NOT.VIS) GO TO 301
      GO TO 300
  301 INS=2*(INT/2)
      IF(INS.LT.2)INS=2
      IP=INS+1
      DELT=DT/INS
      T=.0
      DSZ=CC*DELT
      P11=(.0,.0)
      P12=(.0,.0)
      P21=(.0,.0)
      P22=(.0,.0)
      AMS=AM*AM
      SGN=-1.
      DO 100 IN=1,IP
C   OBSERVATION POINT (X & Y VALUES)
      TX=Y1 + T*CA
      TY=Y1 + T*CB
C
C   X & Y VALUES OF THE TWO SOURCE POINTS ARE XA & YA AND XB & YB.
C
C   DETERMINE IF THE LINE BETWEEN OBSERVATION POINT AND "LEFT" END OF
C   THE SOURCE SEGMENT INTERSECTS THE CYLINDER.
C
      CALL VISIBLE(XA,YA,TX,TY,RADM,AVIS)
C
C   DETERMINE IF THE LINE BETWEEN OBSERVATION POINT AND "RIGHT" END
C   OF THE SOURCE SEGMENT INTERSECTS THE CYLINDER.
      CALL VISIBLE(XB,YB,TX,TY,RADM,BVIS)
      ET11=0.
      ET21=0.
      ET12=0.
      ET22=0.
      IF(AVIS.OR.BVIS) GO TO 701
      GO TO 750
C   OBSERVATION POINT CAN "SEE" AT LEAST ONE OF THE TWO SOURCE SEGMENT
C   END POINTS.
```

Fig. A-2. Subroutine GGSCYL

```
  701 ZZ1=SZ
      ZZ2=SZ - DS
      XXZ=X1+T*CA-XA-SZ*CAS
      YYZ=Y1+T*CB-YA-SZ*CBS
      ZZZ=Z1+T*CG-ZA-SZ*CGS
      RS=XXZ**2+YYZ**2+ZZZ**2
      FAC=1.
      IF(RS.GT.AMS)FAC=(CA*XXZ+CB*YYZ+CG*ZZZ)/RS
      IF(AVIS) GO TO 702
      GO TO 703
C  OBSERVATION POINT CAN "SEE" END POINT A.
  702 R1=SQRT(RS + ZZ1**2)
      EJA=EXP(-GAM*R1)
      EJ1=EJA/R1
      ER11=EJA*SGDS + ZZ1*EJ1*CGDS
      ET11=CC*(-EJ1*CGDS) + FAC*ER11
      ER21= ZZ1*EJ1
      ET21=CC*EJ1 + FAC*ER21
      IF(BVIS) GO TO 703
      GO TO 750
C  OBSERVATION POINT CAN "SEE" END POINT B.
  703 R2=SQRT(RS + ZZ2**2)
          EXP(-GAM*R2)



      EJB=EJB/R2
      ER12= -ZZ2*EJ2
      ET12=CC*EJ2 + FAC*ER12
      ER22=-EJB*SGDS + ZZ2*EJ2*CGDS
      ET22=CC*(-EJ2*CGDS) + FAC*ER22
  750 ET1=ET11 + ET12
      ET2=ET21 + ET22
      C=3.+SGN
      IF(IN.EQ.1 .OR. IN.EQ.2)C=1.
      EGD=EXP(GAM*(DT-T))
      C1=C*(EGD-1./EGD)/2.
      EGD=EXP(GAM*T)
      C2=C*(EGD-1./EGD)/2.
      P11=P11+ET1*C1
      P12=P12+ET1*C2
      P21=P21+ET2*C1
      P22=P22+ET2*C2
      T=T+DELT
      SZ=SZ+DSZ
  100 SGN=-SGN
      CST=-ETA*DELT/(3.*FP*SGDS*SGDT)
      P11=CST*P11
      P12=CST*P12
      P21=CST*P21
      P22=CST*P22
      RETURN
  200 SZ1=(X1-XA)*CAS+(Y1-YA)*CBS+(Z1-ZA)*CGS
      RH1=SQRT((X1-XA-SZ1*CAS)**2+(Y1-YA-SZ1*CBS)**2+(Z1-ZA-SZ1*CGS)**2)
      SZ2=SZ1+DT*CC
      RH2=SQRT((X2-XA-SZ2*CAS)**2+(Y2-YA-SZ2*CBS)**2+(Z2-ZA-SZ2*CGS)**2)
      DDD=(RH1+RH2)/2.
      IF(DDD.GT.20.*AM .AND. INT.GT.0)GO TO 20
      IF(DDD.LT.AM)DDD=AM
      CALL CGMH(.0,DS,SZ1,SZ2,DDD,CGDS,SGDS,SGDT,1.
     2,ETA,GAM,P11,P12,P21,P22)
      RETURN
  300 SS=SQRT(1.-CC*CC)
      CAG=(CGS*CB-CBS*CG)/SS
```

Fig. A-2. (Continued)

```
      CBD=(CAS*CG-CGS*CA)/SS
      CGD=(CBS*CA-CAS*CB)/SS
      DK=(X1-XA)*CAD+(Y1-YA)*CBD+(Z1-ZA)*CGD
      DK=ABS(DK)
      IF(DK.LT.AM)DK=AM
      XZ=XA+SZ*CAS
      YZ=YA+SZ*CBS
      ZZ=ZA+SZ*CGS
      XP1=X1-DK*CAD
      YP1=Y1-DK*CBD
      ZP1=Z1-DK*CGD
      CAP=CBS*CGD-CGS*CBD
      CBP=CGS*CAD-CAS*CGD
      CGP=CAS*CBD-CBS*CAD
      P1=CAP*(XP1-XZ)+CBP*(YP1-YZ)+CGP*(ZP1-ZZ)
      T1=P1/SS
      S1=T1*CC-SZ
      CALL GGMM(S1,S1+DS,T1,T1+DT,DK,CGDS,SGDS,SGDT,CC,ETA,GAM
     2 P11,P12,P21,P22)
      RETURN
      END
```

Fig. A-2. (Continued)

include the x and y end-points of the source and observation segments, as well as the radius of the cylinder in meters. The z values of the end-points are not required since the axis of the cylinder is assumed to lie on the z coordinate axis, as for the cylinder reflection subroutines written by Ekelman. VISIBLE will return the logic variable VIS which will be "FALSE" if the surface of the cylinder intersects a straight line drawn between the source point and the observation point. As with GGS, line 16 will test if the source and observation segments are parallel to each other with small displacement. If so GGSCYL calls GGMM just as GGS does. If closed-form impedance calculations have been selected by the User, which is done by setting variable INT equal to zero, statements 23 thru 26 will determine if the cylinder surface obstructs direct radiation between the two segments. If so, the use of subroutine GGMM is not permitted. If the mutual impedance is to be calculated via Simpson's rule, GGSCYL will again determine if the surface of the cylinder will interfere. At this point, GGSCYL implements the concept introduced by Ekelman in the reflection subroutines SG where the source segment current is considered to be concentrated at points on either end of the source segment as shown in Fig. A-3. The end points of the source segment are labeled A and B for convenience. Subroutine GGSCYL then determines the field which arrives at various points T that lie on the observation segment from the two end points of the source segment, provided that the cylinder surface does not intersect the line between the source segment end point, A or B, and the observation point, T. If it does, the field contribution from that end point is zero. GGSCYL then integrates the received field along the observation

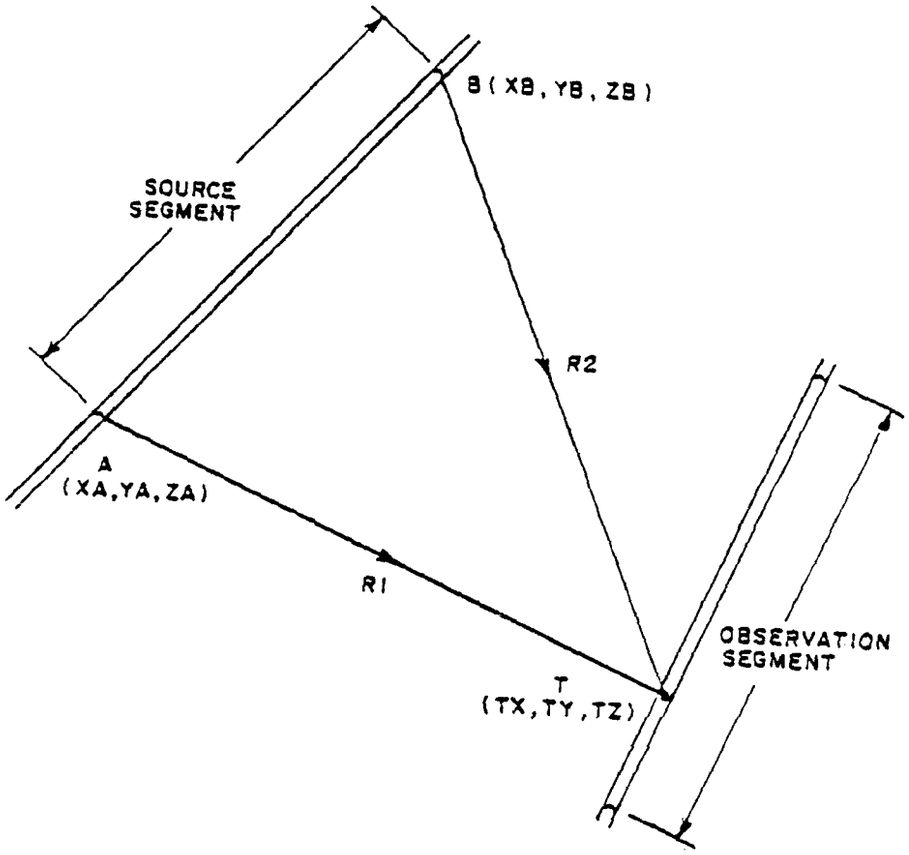

Fig. A-3. Interaction between source and observation segments in subroutine GGSCYL

segment just as the original GGS subroutine does to determine the mutual impedance term for that pair of segments.

Subroutine VISIBLE, listed in Fig. A-4, is frequently called by other subroutines to determine if the surface of a circular cylinder of radius RAD, whose axis is coincident with the z axis, intersects a straight line drawn between points P and R. If the line does not intersect the surface of the cylinder, the logical variable, VIS, is set to a value of "TRUE". Since the problem is independent of the value of z, the cylinder is reduced to a circle in the $z = z_o$ plane. Because of its repeated use by many other subroutine programs, VISIBLE was designed to execute as fast as possible. The geometry of the problem is illustrated in Fig. A-5. First the distance of points P and R from the axis of the cylinder, $|\overline{OP}|$ and $|\overline{OR}|$, is determined and if they are less than the radius, at least one of the points lie inside the cylinder. This is possible for the monopole antenna model used. In that case, the points can not "see" each other and the value of VIS is set to "FALSE". Next, the direction cosines of the line thru P and R are determined. Point Q, which lies on line PR, is determined such that the length of line $|\overline{OQ}|$ represents the minimum distance between the cylinder axis and the line PR. This requires that line OQ be perpendicular to line PR. Using this fact and a theorem from analytical geometry [12] which determines the distance between a plane (or line, sketched as a dashed line in Fig. A-5), normal to a line (PR) that intersects the plane at a point (P), and the origin, the distance $\overline{PQ}$ can be very quickly determined. This allows one to locate point Q. Using the relationship of a right triangle ($\triangle OPQ$) the minimum distance between the line PR and the

```
      SUBROUTINE VISIBLE(PX,PY,RX,RY,RAD,VIS)
C
C  THIS SUBROUTINE DETERMINES IF A STRAIGHT LINE DRAWN THRU POINTS
C  P AND R WILL INTERSECT THE CIRCLE WITH RADIUS A WHOSE CENTER IS
C  AT THE ORIGIN.  IF THE LINE PR DOES NOT INTERSECT THE CIRCLE,


C  THEN "VIS" = "TRUE".
C
      LOGICAL VIS
      REAL LP2,LR2
      LP2=PX*PX + PY*PY
      LR2=RX*RX + RY*RY
      RAD2=RAD*RAD - .00001
      IF(LP2 LT.RAD2 .OR. LR2.LT.RAD2) GO TO 900
      VIS=.TRUE.
C  COMPUTE DIRECTION COSINES THRU P & R.
      DL=SQRT((RX-PX)**2 + (RY-PY)**2)
      IF(DL EQ.0.) RETURN
      C1=(RX-PX)/DL
      C2=(RY-PY)/DL
C  COMPUTE DIRECTION LENGTH OF PERPENDICULAR LEG SP ON LINE PR.
C    (SIMILAR TO SZ CALCULATION IN SBR GGS.)
      SP=-PX*C1 - PY*C2
C  FIND LOCATION OF PERPENDICULAR INTERSECTION Q
      QX= C1*SP + PX
C  TEST IF Q LIES BETWEEN P AND R.
      IF (PX.GT.QX .AND. QX.GT.RX .OR.
     1      RX.GT.QX .AND. QX.GT.PX) GO TO 100
      QY=C2*SP + PY
      IF PY.GT.QY .AND. QY.GT.RY .OR.
     1    RY.GT.QY .AND. QY.GT.PY) GO TO 100
C  CLOSEST POINT TO CYLINDER DOES NOT LIE BETWEEN P AND Q.
      RETURN
C
  100 SP2=SP*SP
C  COMPUTE LENGTH OF PERPENDICULAR LINE FROM LINE PR TO CYLINDER AXIS.
      DP=SQRT(LP2-SP2)
C  DETERMINE IF INTERSECTION WITH CYLINDER OCCURES.
      IF(DP.LE.RAD) VIS=.FALSE.
      RETURN
C  POINT IS INSIDE THE CYLINDER;  OK IF PART OF "MONOPOLE" ANTENNA
C  HOWEVER, POINT MUST NOT BE "VISIBLE" TO OUTSIDE POINTS.
  900 VIS=.FALSE.
      RETURN
      END
```

Fig. A-4. Subroutine VISIBLE

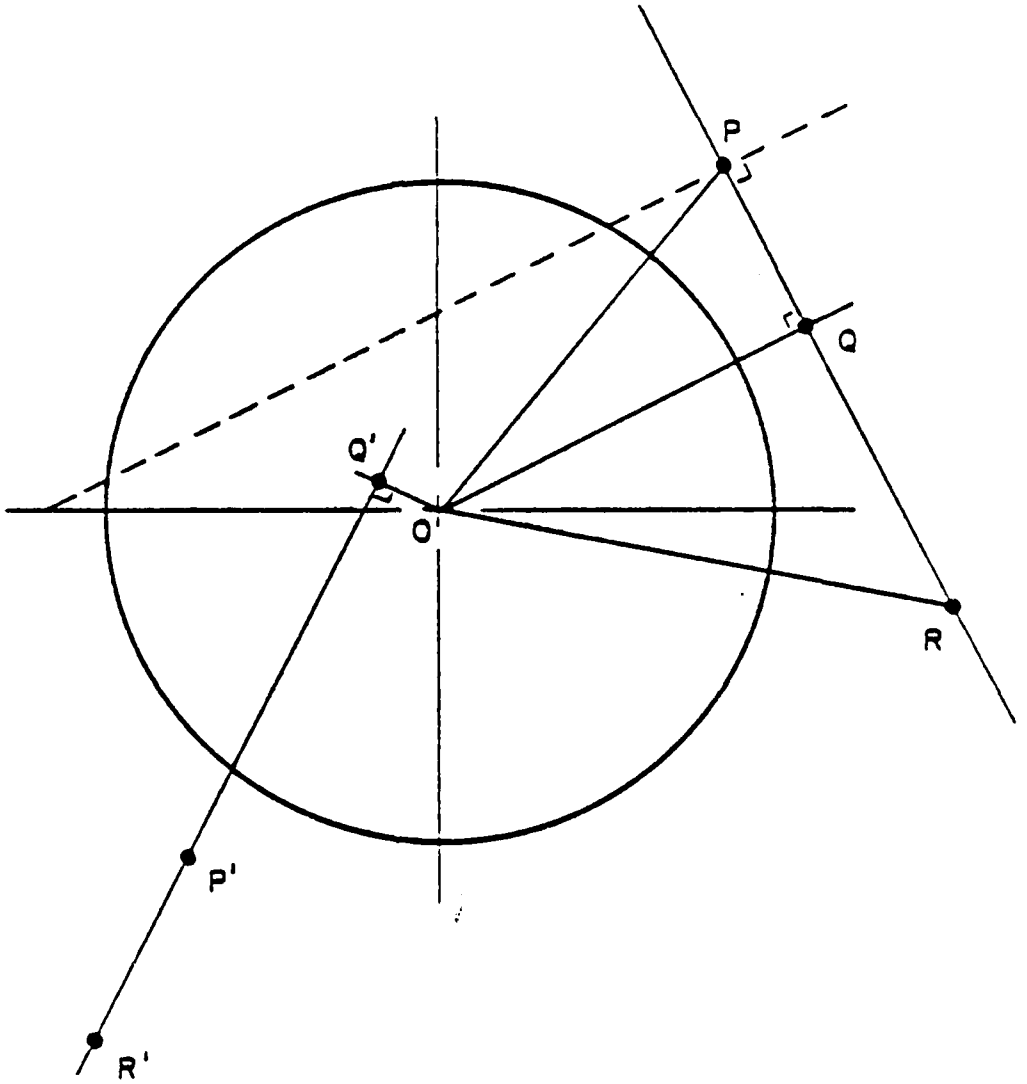

Fig. A-5. Geometry concepts of subroutine VISIBLE

cylinder axis is rapidly computed and compared to the radius of the cylinder. Thus, if the distance $|\overline{OQ}|$ is less than the radius of the cylinder, line PR intersects the cylinder. There is a situation, however, where both points may be located on the same side of the cylinder, as for points P' and R' shown in Fig. A-5. In this case, although line P'R' intersects the cylinder, the cylinder surface does not intersect the line segment between points P' and R' and therefore, P' and R' can still "see" each other. However for this case, point Q', which marks where line P'Q' is closest to the origin, does not lie between the points P' and R'. Thus, in the subroutine, if point Q' does not lie between the two points, and both points are located outside the cylinder (tested at the beginning of VISIBLE), then the two points will be visible to each other, regardless of how close the line thru the two points is to the cylinder axis. This is the purpose of the test at statement 29 of the subroutine.

Subroutine SG determines the delta impedance matrix terms due to reflections from the surface of the cylinder. This subroutine, listed in Fig. A-6, is the routine written by Ekelman except that a call to subroutine VISIBLE is made at statement 159. If the surface of the cylinder is determined to intersect a straight line between the source segment end-point and the observation point, then there is no field which arrives at the observation point due to reflections from the cylinder surface.

Subroutine SGSURF, listed in Fig. A-7, is the subroutine which calculates the delta impedance matrix terms due to boundary-layer surface wave diffraction from the surface of the cylinder. The first

```
      SUBROUTINE SGO(ICJ,IA,IB,INM,INT,ISC,I1,I2,I3,JA,JB,MD,N,ND,NM,
     2EP,AM,BM,C,CGD,CMM,D,EP2,EP3,ETA,FHZ,GAM,SGD,X,Y,Z,ZLD,ZS,A,B,WL)
C * * SGO IS THE SAME AS SG EXCEPT THAT SUBROUTINE "VISIBLE" IS CALLED
C * * TO PRECLUDE COUPLING ANALYSIS BETWEEN TWO SEGMENT POINTS HIDDEN
C * * FROM EACH OTHER BY THE CYLINDER.
      COMPLEX ZG,ZH,ZS,EGD,GD,CGDS,SGDS,SGDT,BØ1
      COMPLEX P11,P12,P21,P22,Q11,Q12,Q21,Q22,EP2,EP,ETA,GAM,EP3
      COMPLEX EPSILA,CWEA,BETA,ZARG
      COMPLEX P(2,2),Q(2,2),CGD(1),SGD(1),C(ICJ,ICJ),ZLD(1)
      COMPLEX EX1,EY1,EZ1,EX2,EY2,EZ2,ETPR,ETPP,PH,ERPR,ERPP
      COMPLEX EX,EY,EZ,ERX,ERY,ERZ,ET1,ET2,EIPR,EIPP,C1,C2,CST
      LOGICAL VIS
      DIMENSION UN(2),UB(2),VI(3)
      DIMENSION X(1),Y(1),Z(1),D(1),IA(1),IB(1),MD(INM,4)
      DIMENSION I1(1),I2(1),I3(1),JA(1),JB(1),ND(1),ISC(1)
      DATA EØ,TP,UØ/8.854E-12,6.28318,1.2566E-6/
      DATA FP/12.56637/
    2 FORMAT(3X,*AM = *,E1Ø.3,3X,*DMAX = *,E1Ø.3,3X,*DMIN = *,E1Ø.3)
C
C        ************************************************
C        *                                              *
C        *  WARNING:                                    *
C        *  SG IS THE ONLY SUBROUTINE WHERE THE VALUE OF *
C        *  THE CYLINDER RADIUS "A" IS IN UNITS OF WAVE  *
C        *  LENGTHS, NOT METERS                         *
C        *                                              *
C        ************************************************
C
      EP=EP3
      ICC=(N*N+N)/2
      DO 11 J=1,N
      DO 1Ø I=1,N
1Ø    C(I,J)=(Ø.,Ø.)
11    CONTINUE
      ZS=(.Ø,.Ø)
      IF(CMM.LE.Ø.)GO TO 12
      OMEGA=TP*FHZ
      EPSILA=CMPLX(EØ,-CMM*1.E6/OMEGA)
      CWEA=(.Ø,1.)*OMEGA*EPSILA
      BETA=OMEGA*SQRT(UØ)*CSQRT(EPSILA-EP)
      ZARG=BETA*AM
      CALL CBES(ZARG,BØ1)
      ZS=BETA*BØ1/CWEA
   12 ZH=ZS/(TP*AM*GAM)
      DMIN=1.E3Ø
      DMAX=.Ø
      DO 2Ø J=1,NM
      K=IA(J)
      L=IB(J)
      D(J)=SQRT((X(K)-X(L))**2+(Y(K)-Y(L))**2+(Z(K)-Z(L))**2)
      IF(D(J).LT.DMIN)DMIN=D(J)
      IF(D(J).GT.DMAX)DMAX=D(J)
      EGD=CEXP(GAM*D(J))
      CGD(J)=(EGD+1./EGD)/2.
   2Ø SGD(J)=(EGD-1./EGD)/2.
      IF(DMIN.LT.2.*AM)GO TO 25
      IF(CABS(GAM*AM).GT.Ø.Ø6)GO TO 25
      IF(CABS(GAM*DMAX).GT.3.)GO TO 25
      IF(AM.GT.Ø.)GO TO 3Ø
   25 N=Ø
      WRITE(6,2)AM,DMAX,DMIN
      RETURN
   3Ø DO 2ØØ K=1,NM
      ND(K)=ND(K)
```

Fig. A-6. Subroutine SG

```
      KA=IA(K)
      KB=IB(K)
      DK=D(K)
      CGDS=CGD(K)
      SGDS=SGD(K)
      DO 200 L=1,NM
      NDL=ND(L)
      LA=IA(L)
      LB=IB(L)
      DL=D(L)
      SGDT=SGD(L)
      NIL=0
      DO 200 II=1,NDK
      I=MD(K,II)
      MM=(I-1)*N-(I*I-I)/2
      FI=1.
      IF(KB.EQ.I2(I))GO TO 36
      IF(KB.EQ.I1(I))FI=-1.
      IS=1
      GO TO 40
   36 IF(KA.EQ.I3(I))FI=-1.
      IS=2
   40 DO 200 JJ=1,NDL
      J=MD(L,JJ)
      MMM=MM+J
C     IF(I.GT.J)GO TO 200
      FJ=1.
      IF(LB.EQ.I2(J))GO TO 46
      IF(LB.EQ.I1(J))FJ=-1.
      JS=1
      GO TO 50
   46 IF(LA.EQ.I3(J))FJ=-1.
      JS=2
   50 IF(NIL.NE.0)GO TO 168
      NIL=1
CC
CC  BEGIN EQUIVALENT TO GGS
CC
      CA=(X(LB)-X(LA))/DL
      CB=(Y(LB)-Y(LA))/DL
      CG=(Z(LB)-Z(LA))/DL
      INS=2*(INT/2)
      IF(INS.LT.2)INS=2
      IP=INS+1
      DELT=DL/INS
      T=0.
      P11=(0.,0.)
      P12=(0.,0.)
      P21=(0.,0.)
      P22=(0.,0.)
      P(1,1)=(0.,0.)
      P(1,2)=(0.,0.)
      P(2,1)=(0.,0.)
      P(2,2)=(0.,0.)
      SGN=-1.
      DO 100 IN=1,IP
      XC=(X(LA)+T*CA)/WL
      YC=(Y(LA)+T*CB)/WL
      ZC=(Z(LA)+T*CG)/WL
      ET1=(0.,0.)
      ET2=(0.,0.)
      DO 102 JEP=1,2
      IF(JEP.EQ.2)GO TO 83
      XSR=X(KA)/WL
```

Fig. A-6. (Continued)

```
      YSR=Y(KA)/WL
      ZSR=Z(KA)/WL
      GO TO 84



   83 XSR=X(KB)/WL
      YSR=Y(KB)/WL
      ZSR=Z(KB)/WL
   84 CONTINUE
C
C  VISIBILITY TEST BETWEEN SOURCE SEGMENT END POINT AND OBSERVATION PT.
C
      CALL VISIBLE(XSR,YSR,XC,YC,A,VIS)
      IF(.NOT.VIS) GO TO 102
CC
CC  RFNPTC FINDS THE REFL PT ON THE CYLINDER
CC
      CALL RFNPTC(XSR,YSR,ZSR,XC,YC,ZC,A,B,XR,YR,ZR,VR,UR,VI,VIM)
CC
CC  GNF FINDS THE FIELD AT THE REFL PT WITH K-SEG AS SOURCE
CC
      XRR=XR*WL
      YRR=YR*WL
      ZRR=ZR*WL
      CALL GNNF(X(KA),Y(KA),Z(KA),X(KB),Y(KB),Z(KB),XRR,YRR,
     2 ZRR,AM,DK,CGDS,SGDS,ETA,GAM,EX1,EY1,EZ1,EX2,EY2,EZ2,JEP)
CC
CC  NANDB FINDS THE NORMAL,BINORMAL,AND TANGENT VECTORS AT REFL PT
CC
      CALL NANDB(A,B,UN,UB,VR)
CC
CC  BEGIN TO FIND FIELD AT XC,YC,ZC DUE TO REFLECTED FIELD AT XR,YR,ZR
CC
      PI=TP/2.
      TPI=TP
      CTHI=UN(1)*VI(1)+UN(2)*VI(2)
      SXN=XSR-XR
      SYN=YSR-YR
      SZN=ZSR-ZR
      SMAG=SQRT(SXN*SXN+SYN*SYN+SZN*SZN)
      SXN=SXN/SMAG
      SYN=SYN/SMAG
      SZN=SZN/SMAG
C  TESTING FOR 0./0. IN ATAN2
      TEMP=SXN*UB(1)+SYN*UB(2)
      IF (TEMP.EQ.0.) GO TO 5
      WR=ATAN2(TEMP,SZN)
      GO TO 6
   5  WR=0.0
   6  SW=SIN(WR)
      CW=COS(WR)
      SST2=SW*SW+CW*CW*CTHI*CTHI
      RHO2=SMAG
      CSV=COS(VR)
      SNV=SIN(VR)
      DD=SQRT(B*B*CSV*CSV+A*A*SNV*SNV)
      RG=DD*DD*DD/A/B
      RHO1=SMAG*RG*CTHI/(RG*CTHI+2.*SMAG*SST2)
      UIPRX=SIN(WR-PI/2.)*UB(1)
      UIPRY=SIN(WR-PI/2.)*UB(2)
      UIPRZ=COS(WR-PI/2.)
      UIPPX=SYN*UIPRZ-SZN*UIPRY
```

Fig. A-6. (Continued)

```
      UIPPY=SZN*UIPPX-SXN*UIPRZ
      UIPPZ=SXN*UIPRY-SYN*UIPPX
      URPPX=UIPRY*V1(3)-UIPRZ*V1(2)
      URPPY=UIPRZ*V1(1)-UIPRX*V1(3)
      URPPZ=UIPRX*V1(2)-UIPRY*V1(1)
      EX=EX1
      EY=EY1


      EZ=EZ1
      DO 101 IMODE=1,2
      EIPR=(UIPRX*EX+UIPRY*EY+UIPRZ*EZ)
      EIPP=(UIPPX*EX+UIPPY*EY+UIPPZ*EZ)
      PH=CEXP(CMPLX(0.,-TPI*VK/SQRT((RHO1+VIM)*(RHO2+VIM))
      ERPR=-SQRT(RHO1*RHO2)*PH*EIPR
      ERPP=SQRT(RHO1*RHO2)*PH*EIPP
      ERX=ERPR*UIPRX+ERPP*UIPPX
      ERY=ERPR*UIPRY+ERPP*UIPPY
      ERZ=ERPR*UIPRZ+ERPP*UIPPZ
CC
CC   DOT THE FIELD WITH THE U-SEG DIRECTION
CC
      IF(IMODE.EQ.1)ET1=ERX*CA+ERY*CB+ERZ*CG+ET1
      IF(IMODE.EQ.2)ET2=ERX*CA+ERY*CB+ERZ*CG+ET2
      EX=EX2
      EY=EY2
  101 EZ=EZ2
  102 CONTINUE
CC
CC   ASSIGN INTEGRATION WEIGHTS AND MODAL CURRENT VALUES
CC
      CWT=3.+SGN
      IF(IN.EQ.1 .OR. IN.EQ.IP)CWT=1.
      EGD=CEXP(GAM*(DL-T))
      C1=CWT*(EGD-1./EGD)/2.
      EGD=CEXP(GAM*T)
      C2=CWT*(EGD-1./EGD)/2.
      P11=P11+ET1*C1
      P12=P12+ET1*C2
      P21=P21+ET2*C1
      P22=P22+ET2*C2
      T=T+DELT
  100 SGN=-SGN
      CST=-DELT/(3.*SGDT)
      P11=CST*P11
      P12=CST*P12
      P21=CST*P21
      P22=CST*P22
      P(1,1)=P11
      P(1,2)=P12
      P(2,1)=P21
      P(2,2)=P22
  168 C(I,J)=C(I,J)+FI*FJ*P(IS,JS)
C     IF(I.NE.J)C(J,I)=C(I,J)
  200 CONTINUE
      RETURN
      END
```

Fig. A-6. (Continued)

```
      SUBROUTINE SGSURF(ICJ,IA,IB,INM,INT,ISC,I1,I2,I3,JA,JB,MD,N,ND,
     1  NM,AM,BM,C,CGD,CMM,D,EP3,ETA,FHZ,GAM,SGD,X,Y,Z,ZLD,
     2  ZS,RADM,WL,NC,FAC)
      COMPLEX CSGDS,EN1,EN2,EMAGS,EMAGL
      COMPLEX ZH,ZS,EGD,CGDS,SGDS,SGDT,BØ1
      COMPLEX P11,P12,P21,P22,EP,ETA,GAM,EP3
      COMPLEX EPSILA,CWEA,BETA,ZARG
      COMPLEX P(2,2),CGD(1),SGD(1),C(ICJ,ICJ),ZLD(1)
      COMPLEX ET1,ET2,C1,C2,CST
      LOGICAL VIS
      DIMENSION NC(1)
      DIMENSION X(1),Y(1),Z(1),D(1),IA(1),IB(1),MD(INM,4)
      DIMENSION I1(1),I2(1),I3(1),JA(1),JB(1),ND(1),ISC(1)
      DATA EØ,TP,UØ/8.854E-12,6.28318,1.2566E-6/
    2 FORMAT(3X,*AM = *,E1Ø.3,3X,*DMAX = *,E1Ø.3,3X,*DMIN = *,E1Ø.3)
      EP=EP3
      DO 11 J=1,N
      DO 1Ø I=1,N
   1Ø C(I,J)=(Ø.,Ø.)
   11 CONTINUE
      ZS=(.Ø,.Ø)
      IF(CMM.LE.Ø.)GO TO 12
      OMEGA=TP*FHZ
      EPSILA=CMPLX(EØ,-CMM*1.E6/OMEGA)
      CWEA=(.Ø,1.)*OMEGA*EPSILA



      BETA=OMEGA*SQRT(UØ)*CSQRT(EPSILA-EP)
      ZARG=BETA*AM
      CALL CBES(ZARG,BØ1)
      ZS=BETA*BØ1/CWEA
   12 ZH=ZS/(TP*AM*GAM)
      DMIN=1.E3Ø
      DMAX=.Ø
      DO 2Ø J=1,NM
      K=IA(J)
      L=IB(J)
      D(J)=SQRT((X(K)-X(L))**2+(Y(K)-Y(L))**2+(Z(K)-Z(L))**2)
      IF(D(J).LT.DMIN)DMIN=D(J)
      IF(D(J).GT.DMAX)DMAX=D(J)
      EGD=CEXP(GAM*D(J))
      CGD(J)=(EGD+1./EGD)/2.
   2Ø SGD(J)=(EGD-1./EGD)/2.
      IF(DMIN.LT.2.*AM)GO TO 25
      IF(CABS(GAM*AM).GT.Ø.Ø6)GO TO 25
      IF(CABS(GAM*DMAX).GT.3.)GO TO 25
      IF(AM.GT.Ø.)GO TO 3Ø
   25 N=Ø
      WRITE(6,2)AM,DMAX,DMIN
      RETURN
   3Ø DO 2ØØ K=1,NM
      NDK=ND(K)
      KA=IA(K)
      KB=IB(K)
      DK=D(K)
      CGDS=CGD(K)
      SGDS=SGD(K)
      CSGDS=-CGDS/SGDS
      DO 2ØØ L=1,NM
      NDL=ND(L)
      LA=IA(L)
      LB=IB(L)
      DL=D(L)
```

Fig. A-7. Subroutine SGSURF

```
      SGDT=SGD(L)
      NIL=Ø
      DO 2ØØ II=1,NDK
      I=MD(K,II)
      MM=(I-1)*N-(I*I-I)/2
      FI=1.
      IF(K3.EQ.I2(I))GO TO 36
      IF(K3.EQ.I1(I))FI=-1.
      IS=1
      GO TO 4Ø
   36 IF(KA.EQ.I3(I))FI=-1.
      IS=2
   4Ø DO 2ØØ JJ=1,NDL
      J=MD(L,JJ)
      I2I=I2(I)
      I2J=I2(J)
      IF(NC(I2I).EQ.Ø .OR. NC(I2J) .EQ.Ø) GO TO 2ØØ
C     IF(I.GT.J)GO TO 2ØØ
      FJ=1.
      IF(LB.EQ.I2(J))GO TO 46
      IF(LB.EQ.I1(J))FJ=-1.
      JS=1
      GO TO 5Ø
   46 IF(LA.EQ.I3(J))FJ=-1.
      JS=2
   5Ø IF(NIL.NE.Ø)GO TO 168
      NIL=1
CC


CC  BEGIN EQUIVALENT TO GGS
CC
C  COMPUTE DIRECTION COSINES OF EXPANSION MODE SEGMENT L
      CA=(X(LB)-X(LA))/DL
      CB=(Y(LB)-Y(LA))/DL
      CG=(Z(LB)-Z(LA))/DL
C  COMPUTE DIRECTION COSINES OF TEST SEGMENT K
      CAS=(X(KB)-X(KA))/DK
      CBS=(Y(KB)-Y(KA))/DK
      CCS=(Z(KB) - Z(KA))/DK
      INT1=INT
      IF( NC(LA).EQ.Ø .AND. NC(KA).EQ.Ø ) INT1=2Ø*INT
      IF( NC(KB).EQ.Ø .AND. NC(LB).EQ.Ø ) INT1=2Ø*INT
      IF( NC(LA).EQ.Ø .AND.NC(KB).EQ.Ø ) INT1=2Ø*INT
      IF( NC(KA).EQ.Ø .AND. NC(LB).EQ.Ø ) INT1=2Ø*INT
      INS=2*(INT1/2)
      IF(INS.LT.2)INS=2
      IP=INS+1
      DELT=DL/INS
      T=Ø.
      P11=(Ø.,Ø.)
      P12=(Ø.,Ø.)
      P21=(Ø.,Ø.)
      P22=(Ø.,Ø.)
      P(1,1)=(Ø.,Ø.)
      P(1,2)=(Ø.,Ø.)
      P(2,1)=(Ø.,Ø.)
      P(2,2)=(Ø.,Ø.)
      SGN=-1.
      DO 1ØØ IN=1,IP
      PX=(X(LA)+T*CA)
      PY=(Y(LA)+T*CB)
      PZ=(Z(LA)+T*CG)
C  LOCATE SOURCE CURRENT AT CENTER OF SOURCE SEGMENT
      PPX=X(KA) + DK*.5*CAS
      PPY=Y(KA) + DK*.5*CBS
      PPZ=Z(KA) + DK*.5*CCS
C
```

```
C  DETERMINE IF P CAN "SEE" PP.  DO NOT COMPUTE SURFACE E-FIELD IF
C  THEY CAN "SEE" EACH OTHER.
C
      CALL VISIBLE(PPX,PPY,PX,PY,RADM,VIS)
      IF(.NOT.VIS) GO TO 261
      EN1=CMPLX(Ø.,Ø.)
      EN2=CMPLX(Ø.,Ø.)
      GO TO 262
  261 CONTINUE
C
C  COMPUTE THE MAGNITUDE OF THE SURFACE FIELDS AT POINT P FROM
C  CURRENTS AT POINT PP.
C
      CALL ESURF(PPX,PPY,PPZ,PX,PY,PZ,RADM,RADM,ETA,GAM,
     1  SPA,CPA,EMAGS,EMAGL,N)
      IF (N.LE.Ø) GO TO 25Ø
C
C  COMPUTE SHORT PATH AND LONG PATH CONTRIBUTIONS FROM MODAL
C  CURRENTS 1 AND 2 AT LEFT END OF THE TEST SEGMENT.
C
C  DOT CURRENT DIRECTION WITH SURFACE NORMAL AT SOURCE POINT PP.
C
      DOT=ABS(CAS*COS(SPA)) + ABS(CBS*SIN(SPA))
C
      EN1=(EMAGS + EMAGL)*DOT*FAC*DK
      EN2=(Ø.,Ø.)



      IF(NDK.NE.1) EN2=EN1
  262 CONTINUE
      CPA=ATAN2(PY,PX)
C
C  DOT THE TOTAL FIELD FOR THIS OBSERVATION POINT WITH THE L-SEGMENT
C  DIRECTION.
C
      ET1=EN1*(ABS(CA*COS(CPA)) + ABS(CB*SIN(CPA)))
      ET2=EN2*(ABS(CA*COS(CPA)) + ABS(CB*SIN(CPA)))
CC
CC  ASSIGN INTEGRATION WEIGHTS AND MODAL CURRENT VALUES
CC
      CWT=3.+SGN
      IF(IN.EQ.1 .OR. IN.EQ.IP)CWT=1.
      EGD=CEXP(GAM*(DL-T))
      C1=CWT*(EGD-1./EGD)/2.
      EGD=CEXP(GAM*T)
      C2=CWT*(EGD-1./EGD)/2.
      P11=P11+ET1*C1
      P12=P12+ET1*C2
      P21=P21+ET2*C1
      P22=P22+ET2*C2
      T=T+DELT
  1ØØ SGN=-SGN
      CST=-DELT/(3.*SGDT)
      P11=CST*P11
      P12=CST*P12
      P21=CST*P21
      P22=CST*P22
      P(1,1)=P11
      P(1,2)=P12
      P(2,1)=P21
      P(2,2)=P22
  168 C(I,J)=C(I,J)+FI*FJ*P(IS,JS)
C     IF(I.NE.J)C(J,I)=C(I,J)
  2ØØ CONTINUE
  25Ø RETURN
      END
```

Fig. A-7. (Continued)

half of the subroutine is the same as for SGANTC or SG. However, unlike SGANTC or SG, the current on the source segment is now considered to be located at the center of the source segment. For a typical, mid-antenna segment, the current distribution is made up of two modal currents as described in Chapter IV. The magnitude of each modal current, previously determined in the main calling program according to the procedure detailed in Chapter IV, is passed to subroutine SGSURF through variable FAC. Thus, the fields ET1 and ET2, arriving at the various observation points, P, on the observation segment are due to current moments with magnitudes equal to FAC, located at the center of the source segment, generated by modal currents I and II on that segment. Subroutine VISIBLE determines if the source segment midpoint, PP, can be "seen" directly by the observation point P. The diffracted field contribution is determined by a call to ESURF only if the two points can not see each other. ESURF will compute the values for EMAGS and EMAGL. EMAGS is the field which arrives at the observation point due to the shortest, most direct path between the source and observation segment, as shown in Fig. 4-3. EMAGL is the field which arrives at the observation point due to the most direct path between the source and observation segment but traveling in the opposite direction around the cylinder as Fig. 4-5 illustrates. Subroutine SGSURF will then add the two fields, EMAGS and EMAGL, as complex numbers, multiply the result by the length of the segment, and take the necessary dot products as required by eqn. (3-1) to account for the orientation of the source and observation segments with respect to the surface of the cylinder.

Subroutine ESURF, listed in Fig. A-8, implements eqn. (3-1). Based on the location of the source point, PP, and the observation point, P, ESURF determines the length of the short and long paths around the cylinder by applying equs. A-1 and A-2 (see Fig. A-9). The pitch angle, δ, is derived, based on eqn. A-3 and eqn. A-4 provided in Fig. A-10. The subroutine computes the other parameters of eqn. (3-1) in a straightforward manner. The hard and soft Fock functions, $F_h(\xi, y_1, y_2)$ and $F_s(\xi, y_1, y_2)$, are evaluated by calling the function subprograms FH and FS respectively.

The function subprograms FH and FS, are listed in Figs. A-11 and A-12. To increase efficiency, the complex values listed in Table 3-1 for τ_n and τ_n' were transformed to rectangular notation and stored in data arrays TN and TPN. The constant coefficients for the hard Fock function residue series (eqns. 3-4 and 3-6) are stored in data array RK in function subprogram FH while the soft Fock function residue series (eqns. 3-5 and 3-7) are contained in data array RKK in function subprogram FS. Data array KV in function subprogram FH stores the constant coefficients for the hard Fock function small argument asymptotic expression terms (eqns. 3-9 and 3-11) and the soft Fock function asymptotic expression coefficients (eqns. 3-10 and 3-12) are stored in data array KU in function subprogram FS.

```
      SUBROUTINE ESURF(PPX,PPY,PPZ,PX,PY,PZ,A,B,ETA,GAM,SPA,CPA,
     1  EMAGS,EMAGL,N)
      COMPLEX ETA,GAM,EMAGS,EMAGL,EMAG1,EMAG2
C
C        * * * * * * * * * * * * * * * * * * * * *
C        *                                       *
C        *  NOTE:  A & B IN THIS SUBROUTINE      *
C        *         ARE IN UNITS OF METERS, NOT   *
C        *         WAVELENGTHS.                  *
C        *                                       *
C        * * * * * * * * * * * * * * * * * * * * *
C
      COMPLEX FH,FHVAL,FS,FSVAL
      COMPLEX J,G
      REAL K
      REAL M
      DATA PI/3.1415926535898/,J/(0.,1.)/
      G(K,S)=K*CEXP(-J*K*S)/(J*PI*2.*S*ETA)
      IF(A.NE.B) GO TO 301
      SNMAG=SQRT(PPX*PPX+PPY*PPY)
      SPA=ATAN2(PPY,PPX)
      CNMAG=SQRT(PX*PX+PY*PY)
      CPA=ATAN2(PY,PX)
      D1=SNMAG-A
      D2=CNMAG-A
      IF(SNMAG.LE.A) D1=0.



      IF(CNMAG.LE.A) D2=0.
C
C  COMPUTE LENGTH OF SHORT PATH AROUND THE CYLINDER FROM NORMAL
C  PROJECTION OF POINT P TO NORMAL PROJECTION OF POINT PP ON THE
C  CYLINDER SURFACE.
C
      SS=SQRT(A*A*(SPA-CPA)**2. + (PPZ-PZ)**2.)
C
C  SIMILARLY, COMPUTE THE LONGER PATH BY GOING THE OTHER WAY AROUND
C  THE CYLINDER BETWEEN THE TWO POINTS.
C
      SL=SQRT(A*A*(2.*PI - ABS(SPA-CPA))**2. + (PPZ-PZ)**2.)
C
C  COMPUTE THE PITCH OF TORSION ANGLES FOR BOTH SHORT AND LONG PATHS.
C
      IF(PPZ-PZ.EQ.0.) GO TO 401
      PSIS=ATAN2(PPZ-PZ,A*(SPA-CPA))
      DELTS=(PI/2.) - ABS(PSIS)
      PSIL=ATAN2(PPZ-PZ,A*((PI*2.) - ABS(SPA-CPA)))
      DELTL=(PI/2.) - ABS(PSIL)
      GO TO 402
  401 DELTS= PI/2.
      DELTL=DELTS
  402 CONTINUE
C
C  COMPUTE THE MAGNITUDE OF THE NORMAL FIELD AT P FOR BOTH THE
C  SHORT AND LONG PATH AROUND THE CYLINDER, STARTING WITH THE SHORT PATH
C
      DELTA=DELTS
      S=SS
      A=ATMAG(GAM)
      DO 100 IPATH=1,2
      IF(DELTA.EQ.0.) GO TO 301
      GO TO 302
  301 EMAG1=(0.,0.)
```

Fig. A-8. Subroutine ESURF

```
      EMAG2=(Ø.,Ø.)
      GO TO 3Ø3
  3Ø2 RHOG=A/(SIN(DELTA)*SIN(DELTA))
      RHOG=A/(SIN(DELTA)*SIN(DELTA))
      M=(K*RHOG/2.)**(1./3.)
      XI=M*S/RHOG
      IF (XI.LE.Ø.) GO TO 9Ø4
      Y1=K*D1/M
      Y2=K*L2/M
      TO=COS(DELTA)
      FHVAL=FH(XI,Y1,Y2)
      FSVAL=FS(XI,Y1,Y2)
      EMAG1=FHVAL - FHVAL*J/(K*S) + FSVAL*(J/(K*S))**2
      EMAG2=(FSVAL - FHVAL)*TO*TO*J/(K*S)
  3Ø3 IF (IPATH EQ.1) GO TO 2Ø1
      EMAG=ETA*ETA*(EMAG1 + EMAG2)*G(K,S)
      GO TO 1ØØ
  2Ø1 EMAGS=ETA*ETA*(EMAG1 + EMAG2)*G(K,S)
      S=SL
      DELTA=DELTL
  1ØØ CONTINUE
      RETURN
C
C  ERROR MESSAGES. N IS USED AS AN ABORT-COMMAND  FLAG.
C
  9Ø1 WRITE(6,6Ø1) A,B
      GO TO 91Ø
  9Ø2 WRITE(6,6Ø2) SNMAG,A
      GO TO 91Ø



  9Ø3 WRITE(6,6Ø3) CNMAG, A
      GO TO 91Ø
  9Ø4 WRITE(6,6Ø4) XI
  91Ø N=-1
      RETURN
  6Ø1 FORMAT(//,*  $$$$ FATAL INPUT DATA ERROR*/
     1  6X,*GEOMETRY EQUATIONS IN THIS ROUTINE ARE VALID*/
     2  6X,*ONLY FOR CIRCULAR CYLINDERS*/
     3  6X,*A = *,E1Ø.3,2X,*B = *,E1Ø.3)
  6Ø2 FORMAT(//,*  $$$$ FATAL INPUT DATA ERROR*/
     1  6X,*SOURCE POINT IS INSIDE THE CYLINDER*/
     2  6X,*SNMAG = *,E1Ø.3,2X,*A = *,E1Ø.3)
  6Ø3 FORMAT(//,*  $$$$ FATAL INPUT DATA ERROR*/
     1 6X,*OBSERVATION POINT IS INSIDE THE CYLINDER*/
     2  6X,*CNMAG = *,E1Ø.3,2X,*A = *,E1Ø.3)
  6Ø4 FORMAT(//,*  $$$$ FATAL INPUT DATA ERROR*/
     1  6X,*XI IS LESS THAN OR EQUAL TO Ø.Ø*/
     2  6X,*XI = *,E1Ø.3)
      END
      COMPLEX FUNCTION FS(XI,Y1,Y2)
C  COMPUTES THE "SOFT"-TYPE FOCK FUNCTION
      COMPLEX J,TN(1Ø),RKK(2),KU(3),KUP(3),SUM
      COMPLEX U, UP
      DATA J/(Ø.,1.)/
      DATA RKK/(2.5Ø6628275,2.5Ø6628275),(3.759942412,3.759942412)/
      DATA TN/(1.169Ø55,-2.Ø24863),(2.Ø43975,-3.54Ø269),
     1  (2.76Ø28,-4.78Ø945),(3.393Ø85,-5.877377),(3.972Ø65,-6.879818),
     2  (4.511325,-7.813844),(5.Ø2Ø1,-8.695Ø68),(5.5Ø425,-9.533641),
     3  (5.965,-10.331683) (6.4144,-11.11ØØ67)/
      DATA KU/ (.626Ø57Ø687,.626657Ø687),(Ø.,.4166666667),
     1  (.Ø97915167,-.Ø97915167)/
      DATA KUP/(-.939985603,-.939985603),(Ø.,1.25),
```

```
     1  (.44Ø6182514,-.44Ø6182514)/
      IF (XI.GT.Ø.6) GO TO 1ØØ
C
C  COMPUTE U AND UP USING THE SMALL ARGUMENT ASYMPTOTIC EXPRESSIONS.
C
      U=1. - KU(1)*XI**1.5 + KU(2)*XI**3  + KU(3)*XI**4.5
      UP=KUP(1)*SQRT(XI) + KUP(2)*XI*XI + KUP(3)*XI**3.5
      GO TO 11Ø
C
C  COMPUTE U AND UP USING THE CONVERGING RESIDUE SERIES IF XI IS
C  GREATER THAN Ø.6
C
  1ØØ SUM=(Ø.,Ø.)
      DO 2ØØ N=1,1Ø
  2ØØ SUM=CEXP(-J*XI*TN(N)) + SUM
      U=REAL(1)*XI**1.5*SUM
      SUM=(Ø.,Ø.)
      DO 21Ø N=1,1Ø
  21Ø SUM=(1-J*XI*TN(N)*2./3.) * CEXP(-J*XI*TN(N)) + SUM
      UP=REAL(2)*SQRT(XI)*SUM
C
C  COMPUTE FS(XI,Y1,Y2) AND RETURN
  11Ø FS=U + J*.5*(UP - 1.5*U/XI)*(Y1*Y1+Y2*Y2)
      RETURN
      END
```

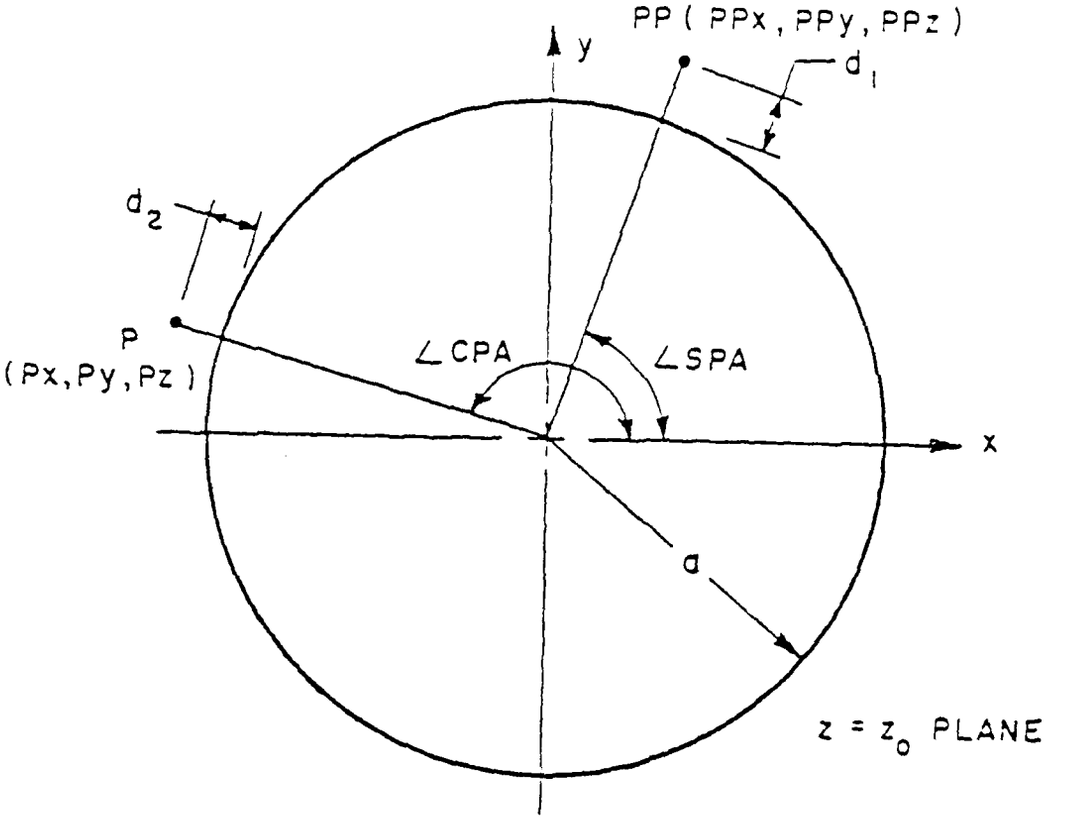

$$(A\text{-}1) \quad SS = \sqrt{a^2 (SPA - CPA)^2 + (z_s - z_c)^2}$$

$$(A\text{-}2) \quad SL = \sqrt{a^2 (2\pi - |SPA - CPA|)^2 + (z_s - z_c)^2}$$

where

$$SPA = \arctan\left(\frac{PPY}{PPX}\right)$$

$$CPA = \arctan\left(\frac{PY}{PX}\right)$$

Fig. A-9. Path length calculations for subroutine ESURF

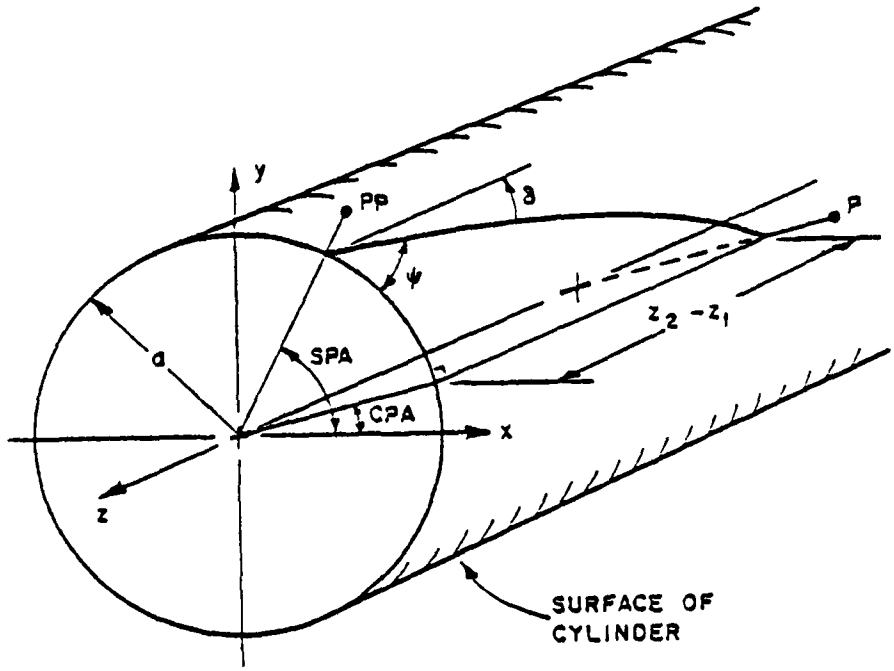

$$\text{(A-1)} \qquad \varphi_s = \arctan \frac{|z_2 - z_1|}{a\,|\mathrm{SPA} - \mathrm{CPA}|}$$

$$\text{(A-2)} \qquad \varphi_\ell = \arctan \frac{|z_2 - z_1|}{a(2\pi - |\mathrm{SPA} - \mathrm{CPA}|)}$$

$$\text{(A-3)} \qquad \delta_{s,\ell} = \frac{\pi}{2} - \varphi_{s,\ell}$$

Fig. A-10. Pitch angle calculations

```
      COMPLEX FUNCTION FS(XI,Y1,Y2)
C  COMPUTES THE "SOL"-TYPE LOCK FUNCTION
      COMPLEX J,TN(10),RES(3),CU(3),CUP(3),SUM
      COMPLEX U, UP
      DATA J/(0.,1.)/
      DATA RES/(2.506628275,2.506628275),(3.759942412,3.759942412)/
      DATA TN/(1.169055,-2.024853),(2.043975,-3.540269),
     1  (2.76428,-4.780945),(3.393305,-5.877377),(3.972486,-6.879818),
     2  (3.511325,-7.813844),(5.0261,-8.695968),(5.504[illegible],-9.5[illegible]),
     3  (6.965,-10.331683),(6.4144,-11.11[illegible])/
      DATA CU/ (.6266570687,.6266570687),(0.,.4166666667),
     1  (.0979151[illegible],-.0979151[illegible])/
      DATA CUP/(-.9399856[illegible],-.9399856[illegible]),(0.,1.25),
     1  (.4466182514,-.4466182514)/
      IF (XI.GT.0.6) GO TO 100
C
C  COMPUTE U AND UP USING THE SMALL ARGUMENT ASYMPTOTIC EXPRESSIONS.
C
      U=1. - CU(1)*XI**1.5 + CU(2)*XI**3. + CU(3)*XI**4.5
      UP=CUP(1)*SQRT(XI) + CUP(2)*XI*XI + CUP(3)*XI**3.5
      GO TO 110
C
C  COMPUTE U AND UP USING THE CONVERGING RESIDUE SERIES IF XI IS
C  GREATER THAN 0.6
C
  100 SUM=(0.,0.)
      DO 200 N=1,10
  200 SUM=CEXP(-J*XI*TN(N)) + SUM
      U=RES(1)*XI**1.5*SUM
      SUM=(0.,0.)
      DO 210 N=1,10
  210 SUM=(1.-J*XI*TN(N)*2./3.) * CEXP(-J*XI*TN(N)) + SUM
      UP=RES(2)*XI**0.5*SUM
C
C  COMPUTE FS(XI,Y1,Y2) AND RETURN
  110 FS=U + J*.5*(UP - 1.5*U/XI)*(Y1*Y1+Y2*Y2)
      RETURN
      END
```

Fig. A-11. Function Subprogram FS

```
      COMPLEX FUNCTION FH(XI,Y1,Y2)
C  COMPUTES THE "HARD"-TYPE FOCK FUNCTION
      COMPLEX J, TPN(10),RK(2),KV(3),KV1(3) SUM
      COMPLEX V,V1
      DATA TPN/(.509395,-.892098),(1.624095,-2.813015),
     1  (2.41005,-4.174329),(3.081695,-5.337583),(3.68609,-6.384495),
     2  (4.244245,-7.351248),(4.767125,-8.257942),(5.26385,-9.117256),
     3  (5.73755,-9.937728),(6.1924,-10.725551)/
      DATA KV/(.3133285343,.3[illegible]85343),(0.,.1166665667),
     1  (.0171351542,.0171351542)/
      DATA KV1/(.6266570687,.6266570687),(0.,.5833333333),
     1  (.1370812338,-.1370812338)/
      DATA J/(0.,1.)/
      DATA RK/(1.253314137,-1.253314137),(2.506628275,2.506628275)/
      IF (XI.GT.0.6) GO TO 100
C
C  COMPUTE V AND V1 USING THE SMALL ARGUMENT ASYMPTOTIC EXPRESSIONS.
C
      V=1. - KV(1)*XI**1.5 + KV(2)*XI**3. + KV(3)*XI**4.5
      V1=1. + KV1(1)*XI**1.5 - KV1(2)*XI**3. - KV1(3)*XI**4.5
      GO TO 110
C
C COMPUTE V AND V1 USING THE CONVERGING RESIDUE SERIES IF XI IS
C  GREATER THAN 0.6
C
  100 SUM=(0.,0.)
      DO 200 N=1,10
  200 SUM=CEXP(-J*XI*TPN(N))/TPN(N) + SUM
      V=RK(1)*SQRT(XI)*SUM
      SUM=(0.,0.)
      DO 210 N=1,10
  210 SUM=CEXP(-J*XI*TPN(N)) + SUM
      V1=RK(2)*XI**1.5*SUM
C
C  COMPUTE FH(XI,Y1,Y2) AND RETURN.
C
  110 FH=V - J*V1*(Y1*Y1 + Y2*Y2)/(4.*XI)
      RETURN
      END
```

Fig. A-12. Function Subprogram FH

REFERENCES

1. G. A. Thiele and T. M. Newhouse, "A Hybrid Technique for Combining Moment Methods with the Geometrical Theory of Diffraction," IEEE Trans. on Antennas and Propagation, Vol. AP-23, No. 1, January 1975.

2. Ernest P. Ekelman, Jr., "A Hybrid Technique for Combining the Moment Method Treatment of Wire Antennas with GTD for Curved Surfaces," Report 710816-1, July 1978, ElectroScience Laboratory, Department of Electrical Engineering, The Ohio State University; prepared under Contract N00014-78-C-0049 for the Office of Naval Research, Arlington, Virginia.

3. J. A. Richmond, "Computer Program for Thin-Wire Structures in a Homogeneous Conducting Medium," NTIS, Springfield, VA 22131, NASA Contractor Report CR-2399, July 1973.

4. W. L. Stutzman and G. A. Thiele, Modern Antenna Theory, John Wiley and Sons, New York, 1980 (in press).

5. P. N. Pathak, W. P. Burnside, and R. J. Marhefka, "A Uniform GTD Analysis of the Scattering of Electromagnetic Waves by a Smooth Convex Surface," Report 784583-4, June 1978, ElectroScience Laboratory, Department of Electrical Engineering, The Ohio State University; prepared for the Naval Air Development Center.

6. P. H. Pathak and N. N. Wang, "An Analysis of the Mutual Coupling Between Antennas on a Smooth Convex Surface," Report 784583-7, October 1978, ElectroScience Laboratory, Department of Electrical Engineering, The Ohio State University; prepared for the Naval Air Development Center.

7. W. D. Burnside, C. L. Yu, and R. J. Marhefka, "A Technique to Combine the Geometrical Theory of Diffraction and the Moment Method," IEEE Trans. on Antennas and Propagation, Vol. AP-23, July 1975, pp. 551-558.

8. J. A. Richmond, "Computer Program for Thin-Wire Structures in a Homogeneous Conducting Medium," Short Course on Application of GTD and Numerical Techniques to the Analysis of Electromagnetic and Acoustic Radiation and Scattering (Text Draft), The Ohio State University, Department of Electrical Engineering, September 1975.

9. J. L. Bogdanor, R. A. Rearlman, and M. D. Siegel, "Intrasystem Electromagnetic Compatibility Analysis Program, Volume I, User's Manual Usage Section," National Technical Information Service, U.S. Department of Commerce, Springfield, Virginia, NTIS No. AD-A008-527, December 1974.

10. C. Hasserjian and A. Ishimaru, "Excitation of a Conducting Cylindrical Surface of Large Radius of Curvature," IRE Transactions on Antennas and Propagation, May 1962, pp. 264-273.

11. J. L. Bogdanor, R. A. Pearlman, and M. D. Siegel, "Intrasystem Electromagnetic Compatibility Analysis Program, Volume I, User's Manual Engineering Section," National Technical Information Service, U.S. Department of Commerce, Springfield, Virginia, NTIS No. AD-A008-526, December 1974.

12. E. J. Purcell, Calculus with Analytic Geometry, Meredith Publishing Co., New York, 1965, pp. 518-519.


DATE
ILME